

A Framework of RIS-assisted ICSC User-centric Based Systems: Latency Optimization and Design

Jiahua Wan, Hong Ren, *Member, IEEE*, Zhiyuan Yu, Zhenkun Zhang, Yang Zhang,
Cunhua Pan, *Senior Member, IEEE*, and Jiangzhou Wang, *Fellow, IEEE*

Abstract—This paper studies a comprehensive framework for reconfigurable intelligent surface (RIS)-assisted integrated communication, sensing, and computation (ICSC) systems with a User-centric focus. The study encompasses two scenarios: the general multi-user equipment (UE) scenario and the simplified single-UE scenario. To satisfy the critical need for time-efficient sensing, we investigate the latency minimization problem, subject to constraints on UEs' transmit power, radar signal-to-interference-plus-noise-ratio (SINR), RIS phase shift, and computation capability. To address the formulated non-convex problem in the multi-UE scenario, we decouple the original problem into two subproblems, where the computational and beamforming settings are optimized alternately. Specifically, for the computational settings, we derive a closed-form solution for the offloading volume and propose a low-complexity algorithm based on the bisection search method to optimize the edge computing resource allocation. Additionally, we employ two equivalent transformations to address the challenge posed by the non-convex sum-of-ratios form in the objective function (OF) of the subproblem related to active and passive beamforming. Several techniques are then combined to address these subproblems. Furthermore, a low-complexity algorithm that offers closed-form solutions is developed for the simplified single UE scenario. Finally, simulation results substantiate the effectiveness of the proposed framework.

Index Terms—Integrated communication, sensing, and computation (ICSC), dual function radar and communication (DFRC), reconfigurable intelligent surface (RIS), mobile edge computing (MEC)

I. INTRODUCTION

WITH THE ADVENT OF sixth-generation (6G) networks, the explosion in the number of user equipments (UEs) in wireless communication has precipitated a severe scarcity of spectrum resources [2]. Integrated sensing and communication (ISAC) has emerged as a pivotal 6G technology, efficiently fulfilling both communication and sensing functions within the same frequency band, thereby enhancing spectral efficiency [3]–[5].

However, the efficient processing of vast distributed ISAC data remains a formidable challenge, necessitating innovative solutions such as the integration of mobile edge computing (MEC) [6] with ISAC. Specifically, MEC facilitates the migration of computation capability to the wireless network edge

by deploying edge servers at cellular base stations (BSs), as demonstrated in [7]. This strategic placement enables the execution of high computational tasks in proximity to ISAC application, thereby achieving ultra-low ISAC service latency while minimizing traffic loads. This integration paves the way for integrated communication, sensing, and computation (ICSC), which strategically processes high computational tasks at the network edge, thereby reducing latency and network congestion significantly [8]–[11].

Nonetheless, the efficacy of ICSC systems can be compromised owing to the potential obstacles in practical scenarios, which may lead to prolonged offloading delays in MEC [12] and diminished received power of sensing signals [13], [14]. Fortunately, reconfigurable intelligent surfaces (RISs) can address these challenges by dynamically adjusting the phase of incident electromagnetic waves [15]–[17], thus enhancing both communication and sensing capabilities in ISAC systems [18], [19]. Furthermore, RIS is able to reduce delays by establishing additional reliable links and improving channel quality [20]–[22]. According to the above-mentioned benefits of the deployment of the RIS, it is considered as well-suited for integration into ICSC systems to enhance their overall performance and reliability. Consequently, researchers have been inspired to investigate the performance of RIS-assisted ICSC systems [23], [24]. In particular, [23] utilized the RIS to alleviate interference between the radar and the edge computing server (ECS), proposing an energy-efficient system. Meanwhile, the authors of [24] employed the RIS as a passive information source in an ICSC system and maximized the weighted throughput capacity, which was considered as a metric for performance evaluation.

However, both [23] and [24] considered ICSC systems deployed predominantly at the base station (BS) end, aligning with the BS-centric model where BSs are tasked with probing sensing signals, and UEs are responsible for offloading information to these BSs. This arrangement, as elaborated in [25], enhances efficient signal interference management and optimizes network resources. However, the BS-centric based ICSC systems may not fully cater to scenarios requiring rapid response and decentralized processing capabilities. In contrast, the User-centric based ICSC systems [26]–[28] are capable of addressing these limitations by enabling UEs not only to engage in sensing tasks but also to process these tasks directly. This approach fosters high hardware sharing, thereby boosting spectrum and energy efficiency.

Owing to the well-suited nature of RIS to ICSC systems and the advantages of User-centric based ICSC systems, it is

Part work of this article was accepted by the IEEE International Conference on Acoustics, Speech and Signal Processing Workshops (ICASSPW), Seoul, Korea, April 2024 [1].

J. Wan, H. Ren, Z. Yu, Z. Zhang, Y. Zhang, and C. Pan are with National Mobile Communications Research Laboratory, Southeast University, Nanjing, China. (email: {wanjiahua, hren, zyyu, zhenkun_zhang, y_zhang, cpan}@seu.edu.cn). J. Wang is with the School of Engineering, University of Kent, Canterbury CT2 7NT, U.K. (e-mail: j.z.wang@kent.ac.uk).

critical to investigate the RIS-assisted User-centric ICSC systems. This integration not only ensures low latency and high performance of ICSC systems but also contributes to boosting spectrum and energy efficiency. Specifically, RIS enhances the communication link of the ICSC system and facilitates the offloading of the substantial volume of data generated by the radar sensing to the ECS, thus ensuring the low latency attainment of the highly accurate sensing results. However, to the best of our knowledge, research on this integration is still missing.

While we recognize the significant importance, studying the RIS-assisted User-centric based ICSC systems is indeed a highly challenging task. Firstly, compared to the BS-centric [25], the User-centric approach inherently involves a wider variety of scenarios compared to the BS-centric model, increasing the difficulty due to the diversity and unpredictability of user environments and behaviors. Interference among UEs significantly affects the sensing and communication functionalities in ICSC systems, complicating the overall allocation of computational resources and the optimization of system performance. Additionally, when considering a more general case such as multi-input multi-output (MIMO), the challenges intensify. From a technical perspective, the incorporation of precoding in the form of matrices for MIMO scenarios presents significant challenges in processing the performance matrices in ICSC systems. This complexity is due to the need to optimize multiple spatial streams simultaneously, which requires intricate balancing of signal integrity across various channels and users within the User-centric ICSC framework. Furthermore, within this framework, it is crucial to address the challenge separately for both the multi-UE and single-UE scenarios, a topic that has not yet been explored in the literature. Thus, the methods proposed in prior works [29], [30] cannot be directly adopted.

Inspired by the preceding discussion, this paper delves into a framework for RIS-assisted ICSC systems with a User-centric focus, where the RIS is deployed to facilitate the offloading of the computing data to the ECS. For the multi-UE scenario, we propose a block coordinate descent (BCD)-based algorithm that integrates the minimum variance distortionless response (MVDR), successive convex approximation (SCA), majorization-minimization (MM), and weighted minimum mean-square error (WMMSE) to effectively address the challenges identified within the system. Then, for the simplified single-UE scenario, a low-complexity algorithm that yields closed-form solutions is presented. The main contributions of this paper are summarized as follows:

- **New User-centric Framework:** An RIS-assisted ICSC system within a User-centric DFRC framework is investigated, where multiple DFRC-enabled UEs simultaneously detect targets and upload radar-sensing computational tasks to an ECS through their communication functionalities. Specifically, we jointly optimize the precoding and decoding matrices of the uplink signal, the receive radar beamforming vector, the RIS phase shift vector, the offloading volume, and the edge computational resource allocation to minimize the weighted latency. Due to the highly coupling among the variables, a BCD-based algo-

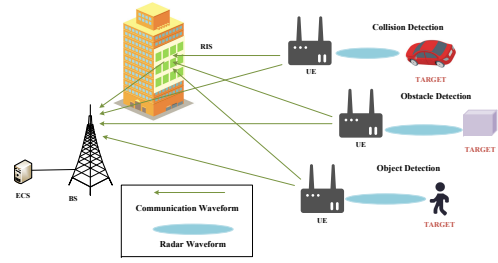


Fig. 1. System model.

gorithm is proposed to effectively decouple the optimization of the computational settings and the active and passive beamforming matrices into two subproblems.

- **Comprehensive solution for multi-UE scenario:** For the computational settings, we employ the BCD technique again to decouple the offloading volume and the edge computing resource allocation. When the allocation of edge computing resources is fixed, the optimal computational offloading can be determined under the assumption that the latencies of local and edge computing are equal. Given the computational offloading, the Karush-Kuhn-Tucker (KKT) conditions and the bisection search method are employed to determine the optimal allocation of edge computing resources. Then, with fixed computing design, we deal with the joint optimization problem of active and passive beamforming, the objective function (OF) of which takes the form of a non-convex sum-of-ratios, presenting a significant challenge. To address this issue, we reformulate the OF into a tractable form of a weighted sum-rate by introducing auxiliary variables and subsequently develop an iterative algorithm to solve it. In each iteration, the auxiliary variables are updated using the modified Newton's method. Following the reformulation of the objective function with the WMMSE algorithm, the MVDR, SCA, and MM techniques are employed to optimize the the receive radar beamforming vector, the precoding matrices of the uplink signal and the RIS phase shift vector, respectively.
- **Close-form Solution for Single-UE Scenario:** Furthermore, a specific scenario involving a single UE is examined, where the edge computational resource allocation and interference from multiple UEs are not taken into account. We derive a closed-form solution in each iteration.
- **Effectiveness of the Framework:** Simulation results verify the effectiveness of the proposed algorithms and the advantages of employing the RIS-assisted ICSC system. It is demonstrated that the proposed algorithm significantly improves the latency performance of the ISCC system in comparison to the conventional approach that lacks an integrated RIS.

Notation: Throughout this paper, scalars, vectors, and matrices are denoted by lowercase italicized letters, lowercase bold letters, and uppercase bold letters, respectively. $\mathbb{C}^{N \times M}$ denotes the space of $N \times M$ complex matrices. $(\cdot)^T$, $(\cdot)^*$, and $(\cdot)^H$ denote the transpose, complex conjugation, and Hermi-

tian operators, respectively. $(\cdot)^*$ represents the optimal result of a variable. $\text{Tr}(\cdot)$ is the trace of a matrix. $\mathbb{E}(\cdot)$ denotes the statistical expectation operation. $\lfloor \cdot \rfloor$ and $\lceil \cdot \rceil$ are the floor and ceiling of a scalar, respectively. $\text{Re}\{\cdot\}$ and $\angle(\cdot)$ represent the real part and the argument of a complex number. \odot denotes the Hadamard product of two matrices. $\text{diag}\{\mathbf{x}\}$ means the diagonal matrix where the diagonal elements are \mathbf{x} . $|\cdot|$ and $\|\cdot\|$ represent the absolute value of a scalar and the Euclidean norm of a vector, respectively.

II. SYSTEM MODEL AND PROBLEM FORMULATION

A. Communication Model

Consider an RIS-assisted ICSC system as illustrated in Fig. 1, which consists of K DFRC-enabled UEs with N antennas, an L -element RIS, and an M -antenna BS connected to an ECS.¹ Each UE is capable of simultaneously conducting target sensing and communicating with the BS to exchange crucial information and facilitate centralized control. The UE offloads data to the BS via the communication function and enable the rapid acquisition of sensing results with improved accuracy. Since UEs and their corresponding targets are spatially separated from the BS, it is assumed that the RIS is dedicated to providing support for edge computing and does not impact the sensing capabilities of the UEs [31]. By defining the precoding matrix as $\mathbf{F}_{c,k} \in \mathbb{C}^{N \times d}$ and the transmit symbols at time slot n as $\mathbf{c}_k = [c_{k,1}[n], \dots, c_{k,d}[n]]^T \in \mathbb{C}^{d \times 1}$, satisfying $\mathbb{E}[\mathbf{c}_k \mathbf{c}_k^H] = \mathbf{I}_d$ and $\mathbb{E}[\mathbf{c}_k \mathbf{c}_l^H] = \mathbf{0}_d$, the transmit signal of UE k is expressed as

$$\mathbf{x}_k = \mathbf{F}_{c,k} \mathbf{c}_k \in \mathbb{C}^{N \times 1}. \quad (1)$$

We denote the channels from UE k to the BS, from the RIS to the BS, and from UE k to the RIS by $\mathbf{H}_{\text{bu},k} \in \mathbb{C}^{M \times N}$, $\mathbf{H}_{\text{r}} \in \mathbb{C}^{M \times L}$, and $\mathbf{H}_{\text{ru},k} \in \mathbb{C}^{L \times N}$, respectively. For simplicity, the reflection elements of the RIS have unit amplitude and thus the reflecting coefficients matrix of the RIS can be expressed as $\mathbf{V} = \text{diag}\{e^{j\theta_1}, \dots, e^{j\theta_L}\} \in \mathbb{C}^{L \times L}$, where $\theta_l \in (0, 2\pi]$, $\forall l \in \mathcal{L} = \{1, \dots, L\}$ is the phase of the l -th reflecting element of RIS. The overall channel matrix between UE k and the BS is given by

$$\mathbf{H}_k \triangleq \mathbf{H}_{\text{bu},k} + \mathbf{H}_{\text{r}} \mathbf{V} \mathbf{H}_{\text{ru},k} \in \mathbb{C}^{M \times N}. \quad (2)$$

Then, the signal vector received at the BS is formulated as

$$\mathbf{y}_c = \sum_{k=1}^K \mathbf{H}_k \mathbf{F}_{c,k} \mathbf{c}_k + \mathbf{n}_c \in \mathbb{C}^{M \times 1}, \quad (3)$$

where $\mathbf{n}_c = [n_{c,1}, \dots, n_{c,M}]^T \in \mathbb{C}^{M \times 1}$, which satisfies $\mathbf{n}_c \sim \mathcal{CN}(\mathbf{0}, \sigma_c^2 \mathbf{I}_M)$, denotes the additive white Gaussian noise (AWGN) at the BS. After decoding the received signal with a linear matrix $\mathbf{W}_{c,k}$, we can obtain the recovered signal of UE k as

$$\begin{aligned} \hat{\mathbf{c}}_k &= \mathbf{W}_{c,k}^H \mathbf{y}_c \\ &= \mathbf{W}_{c,k}^H \left(\sum_{k=1}^K \mathbf{H}_k \mathbf{F}_{c,k} \mathbf{c}_k + \mathbf{n}_c \right) \in \mathbb{C}^{d \times 1}. \end{aligned} \quad (4)$$

¹The radar sensing process generates a substantial volume of computation-intensive data, an ECS is situated at the BS to expedite the processing of the radar data.

The covariance of the transmit signal from UE k is given by

$$\mathbf{R}_{\mathbf{x},k} \triangleq \mathbb{E}[\mathbf{x}_k \mathbf{x}_k^H] = \mathbf{F}_{c,k} \mathbf{F}_{c,k}^H. \quad (5)$$

By denoting the transmit power of UE k by $P_{t,k}$, the power constraint for UE k is expressed as

$$\text{Tr}(\mathbf{R}_{\mathbf{x},k}) = \text{Tr}(\mathbf{F}_{c,k} \mathbf{F}_{c,k}^H) \leq P_{t,k}, \forall k \in \mathcal{K} = \{1, \dots, K\}. \quad (6)$$

Furthermore, the achievable off-loading rate (bit/s/Hz) of UE k can be formulated as

$$\begin{aligned} R_k(\mathbf{F}_c, \mathbf{W}_{c,k}, \boldsymbol{\theta}) \\ = B_\omega \log_2 |\mathbf{I}_d + \mathbf{W}_{c,k}^H \mathbf{H}_k \mathbf{F}_{c,k} \mathbf{F}_{c,k}^H \mathbf{H}_k^H \mathbf{W}_{c,k} (\mathbf{W}_{c,k}^H \mathbf{J}_k \mathbf{W}_{c,k})^{-1}|, \end{aligned} \quad (7)$$

where B_ω denotes the bandwidth, $\boldsymbol{\theta}$ is defined as $\boldsymbol{\theta} = [\theta_1, \dots, \theta_L]$, and \mathbf{J}_k represents the interference plus noise matrix of UE k that is given by

$$\mathbf{J}_k = \sum_{i=1, i \neq k}^K \mathbf{H}_i \mathbf{F}_{c,i} \mathbf{F}_{c,i}^H \mathbf{H}_i^H + \sigma_c^2 \mathbf{I}_M \in \mathbb{C}^{M \times M}.$$

B. Radar Sensing Model

Given the transmit signal \mathbf{x}_k in (1), the received echo of UE k is expressed as²

$$\mathbf{y}_{s,k} = \alpha_k \mathbf{a}_{\text{R},k}(\theta_k) \mathbf{a}_{\text{T},k}^H(\theta_k) \mathbf{x}_k + \sum_{i=1, i \neq k}^K \mathbf{H}_{k,i} \mathbf{x}_i + \mathbf{z}_k \in \mathbb{C}^{N \times 1}, \quad (8)$$

where α_k represents the amplitude of the radar target located at angle θ_k , $\mathbf{a}_{\text{R},k}(\theta_k) \in \mathbb{C}^{N \times 1}$ and $\mathbf{a}_{\text{T},k}(\theta_k) \in \mathbb{C}^{N \times 1}$ are the receive and transmit array response vectors for UE k , respectively. Matrix $\mathbf{H}_{k,i} \in \mathbb{C}^{N \times N}$ denotes the channel matrix between UE k and UE i , and $\mathbf{z}_k = [z_{k,1}, \dots, z_{k,N}]^T \in \mathbb{C}^{N \times 1}$ is the AWGN with the covariance of σ_s^2 . For simplicity, we define $\mathbf{G}_k \triangleq \alpha_k \mathbf{a}_{\text{R},k}(\theta_k) \mathbf{a}_{\text{T},k}^H(\theta_k) \in \mathbb{C}^{N \times N}$ as the target response matrix. Then, the radar output at UE k is given by

$$r_k = \mathbf{w}_{s,k}^H \mathbf{G}_k \mathbf{x}_k + \sum_{i=1, i \neq k}^K \mathbf{w}_{s,k}^H \mathbf{H}_{k,i} \mathbf{x}_i + \mathbf{w}_{s,k}^H \mathbf{z}_k, \quad (9)$$

where $\mathbf{w}_{s,k} \in \mathbb{C}^{N \times 1}$ is the receive beamforming vector of UE k .

The sensing performance can be measured in terms of the radar SINR. After applying receive beamforming, the radar SINR for UE k , denoted by γ_k , is given by

$$\begin{aligned} \gamma_k &= \frac{\mathbb{E} \left[|\mathbf{w}_{s,k}^H \mathbf{G}_k \mathbf{x}_k|^2 \right]}{\mathbb{E} \left[|\mathbf{w}_{s,k}^H (\sum_{i=1, i \neq k}^K \mathbf{H}_{k,i} \mathbf{x}_i + \mathbf{z}_k)|^2 \right]} \\ &= \frac{\text{Tr}(\mathbf{w}_{s,k}^H \mathbf{G}_k \mathbf{F}_{c,k} \mathbf{F}_{c,k}^H \mathbf{G}_k^H \mathbf{w}_{s,k})}{\text{Tr}(\mathbf{w}_{s,k}^H \mathbf{T}_k \mathbf{w}_{s,k})}, \end{aligned} \quad (10)$$

where $\mathbf{T}_k \triangleq \sum_{i=1, i \neq k}^K \mathbf{H}_{k,i} \mathbf{F}_{c,i} \mathbf{F}_{c,i}^H \mathbf{H}_{k,i}^H + \sigma_s^2 \mathbf{I}_N \in \mathbb{C}^{N \times N}$.

²Note that the radar clutter can be effectively mitigated or eliminated through radar signal processing techniques, we disregard the effects of clutter as [28]. Thus, the radar and computational offloading performance achieved by the proposed algorithms can be regarded as theoretical upper bounds.

C. Computation Model

The partial off-loading strategy is adopted for computational tasks, where a fraction of the data is processed locally, while the remaining portion is offloaded to the BS.

a) *Local Computation Model*: For UE k , we denote the overall number of bits awaiting processing, the number of bits designated for offloading, the number of CPU cycles required for processing each bit, and its CPU frequency by V_k, v_k, c_k , and f_k^l , respectively. Then, the latency for local computation of UE k is given by $T_{1,k} = (V_k - v_k)c_k/f_k^l$.

b) *Edge Computation Model*: Let f_k^e with $\sum_{k=1}^K f_k^e \leq f_{\text{total}}^e$ denote the computation resources allocated to UE k , where f_{total}^e represents the processing rate of the ECS. It is assumed that the edge computing process for UE k begins when all v_k offloaded bits are received at the BS. The entire process of edge computation for UE k can be divided into three steps: computing offloading, edge computing, and result feedback, with the feedback latency typically being neglected [32]. Consequently, the total latency of edge computation for UE k is expressed as $T_{c,k} = T_{o,k} + T_{e,k} = v_k/R_k(\mathbf{F}_c, \mathbf{W}_{c,k}, \boldsymbol{\theta}) + v_k c_k/f_k^e$.

We consider the simultaneous execution for local and edge computation. In this case, the latency of UE k can be represented by

$$\begin{aligned} T_k(\mathbf{F}_c, \mathbf{W}_{c,k}, \boldsymbol{\theta}, v_k, f_k^e) &= \max\{T_{1,k}, T_{c,k}\} \\ &= \max\left\{\frac{(V_k - v_k)c_k}{f_k^l}, \frac{v_k}{R_k(\mathbf{F}_c, \mathbf{W}_{c,k}, \boldsymbol{\theta})} + \frac{v_k c_k}{f_k^e}\right\}. \end{aligned} \quad (11)$$

D. Problem Formulation

In this paper, we aim to minimize the total weighted latency of all UEs by jointly optimizing the communication precoding matrices $\mathbf{F}_c = \{\mathbf{F}_{c,k}, \forall k \in \mathcal{K}\}$, the communication decoding matrices $\mathbf{W}_c = \{\mathbf{W}_{c,k}, \forall k \in \mathcal{K}\}$, the receive radar beamforming vectors $\mathbf{w}_s = \{\mathbf{w}_{s,k}, \forall k \in \mathcal{K}\}$, the RIS phase shift vector $\boldsymbol{\theta} = [\theta_1, \dots, \theta_L]$, the offloading volume $\mathbf{v} = [v_1, \dots, v_K]^T$, and the edge computational resource allocation $\mathbf{f} = [f_1^e, \dots, f_K^e]^T$. The optimization problem is formulated as

$$\mathcal{P}0: \min_{\mathbf{F}_c, \mathbf{W}_c, \mathbf{w}_s, \boldsymbol{\theta}, \mathbf{v}, \mathbf{f}} \sum_{k=1}^K \xi_k T_k(\mathbf{F}_c, \mathbf{W}_{c,k}, \boldsymbol{\theta}, v_k, f_k^e) \quad (12a)$$

$$s.t. \quad \text{Tr}(\mathbf{R}_{\mathbf{x},k}) \leq P_{t,k}, \forall k \in \mathcal{K}, \quad (12b)$$

$$\gamma_k \geq \eta, \forall k \in \mathcal{K}, \quad (12c)$$

$$0 < \theta_l \leq 2\pi, \forall l \in \mathcal{L}, \quad (12d)$$

$$\sum_{k=1}^K f_k^e \leq f_{\text{total}}^e, \quad (12e)$$

$$v_k \in \{0, 1, \dots, V_k\}, \forall k \in \mathcal{K}, \quad (12f)$$

$$f_k^e \geq 0, \forall k \in \mathcal{K}, \quad (12g)$$

where ξ_k represents the weight of UE k and η denotes the radar SINR requirement of UEs. The constraints (12e) - (12g) are introduced based on the computation model in Sec. II-C.

Addressing Problem $\mathcal{P}0$ poses several challenges. Firstly, the OF of Problem $\mathcal{P}0$ is in a segmented form. Secondly, the variables of Problem $\mathcal{P}0$ are highly coupled. Finally, the

weighted total latency involves calculating the sum of ratios, which can often be challenging to optimize.

III. ALGORITHM DESIGN

In this section, Problem $\mathcal{P}0$ is decoupled into multiple sub-problems by using the BCD method, for which solutions are subsequently devised.

A. Joint Optimization of Offloading Volume \mathbf{v} and Edge Computing Resource Allocation \mathbf{f}

Given $\{\mathbf{F}_c, \mathbf{W}_c, \mathbf{w}_s, \boldsymbol{\theta}\}$, Problem $\mathcal{P}0$ is reformulated as

$$\begin{aligned} \mathcal{P}1: \min_{\mathbf{v}, \mathbf{f}} \quad & \sum_{k=1}^K \xi_k T_k(v_k, f_k^e) \\ s.t. \quad & (12e), (12f), (12g). \end{aligned} \quad (13)$$

It can be verified that $T_{1,k}$ and $T_{c,k}$ are respectively monotonically decreasing and increasing with respect to (w.r.t.) v_k . Therefore, given \mathbf{f} , the minimum value of $T_k(v_k) = \max\{T_{1,k}, T_{c,k}\}$ is obtained when $T_{1,k} = T_{c,k}$ is satisfied. Accordingly, the value of v_k that minimizes $T_k(v_k)$ without the integer constraint, denoted by \hat{v}_k^* , is given by

$$\hat{v}_k^* = \frac{V_k c_k R_k f_k^e}{f_k^e f_k^l + c_k R_k (f_k^e + f_k^l)}, \forall k \in \mathcal{K}. \quad (14)$$

Therefore, the optimal value of v_k is obtained according to

$$v_k^* = \arg \min_{\hat{v}_k \in \{\lfloor \hat{v}_k^* \rfloor, \lceil \hat{v}_k^* \rceil\}} T_k(\hat{v}_k), \forall k \in \mathcal{K}. \quad (15)$$

Given \mathbf{v} , Problem $\mathcal{P}1$ can be rewritten as follows:

$$\begin{aligned} \mathcal{P}1-1: \min_{\mathbf{f}} \quad & \sum_{k=1}^K \xi_k \frac{V_k c_k^2 R_k + V_k c_k f_k^e}{f_k^e f_k^l + c_k R_k (f_k^e + f_k^l)} \\ s.t. \quad & (12e), (12g). \end{aligned} \quad (16)$$

Problem $\mathcal{P}1-1$ is convex w.r.t. \mathbf{f} and satisfies the Slater's condition [33]. Hence, the optimal solution of Problem $\mathcal{P}1-1$ can be derived via the KKT conditions. Specifically, the Lagrangian function of Problem $\mathcal{P}1-1$ can be formulated as

$$\mathcal{L}(\mathbf{f}, \mu) = \sum_{k=1}^K \xi_k \frac{V_k c_k^2 R_k + V_k c_k f_k^e}{f_k^e f_k^l + c_k R_k (f_k^e + f_k^l)} + \mu \left(\sum_{k=1}^K f_k^e - f_{\text{total}}^e \right), \quad (17)$$

where $\mu \geq 0$ denotes the Lagrange multiplier. Furthermore, the KKT conditions for Problem $\mathcal{P}1-1$ are expressed as

$$\frac{\partial \mathcal{L}}{\partial f_k^e} = \frac{-\xi V_k c_k^3 R_k^2}{[c_k R_k f_k^l + (f_k^l + c_k R_k) f_k^{e*}]^2} + \mu^* = 0, \quad (18)$$

$$\mu^* \left(\sum_{k=1}^K f_k^{e*} - f_{\text{total}}^e \right) = 0, \quad (19)$$

$$f_k^{e*} \geq 0. \quad (20)$$

Given μ , we can obtain the value of f_k^{e*} by solving (18) as

$$f_k^{e*} = \sqrt{\frac{\xi V_k c_k^3 R_k^2}{\mu^*} - c_k R_k f_k^l}, \forall k \in \mathcal{K}. \quad (21)$$

From (20), we have $\sqrt{\frac{\xi V_k c_k^3 R_k^2}{\mu^*} - c_k R_k f_k^l} \geq 0$, and thus $\mu^* \leq \frac{\xi V_k c_k}{f_k^{l2}}$. Consequently, the value μ^* is within the range

Algorithm 1 Joint optimization of $\{\mathbf{v}, \mathbf{f}\}$, given $\{\mathbf{F}_c, \mathbf{W}_c, \mathbf{w}_s, \boldsymbol{\theta}\}$

- 1: Initialize iteration number $t_1 = 0$. Set the maximum number of iterations to t_1^{\max} . Initialize $\mathbf{f}^{(0)}$ satisfying (12e) and (12g).
- 2: **Repeat**
- 3: Calculate $\mathbf{v}^{(t_1+1)}$ using (14).
- 4: Calculate μ and $\mathbf{f}^{(t_1+1)}$ accordingly using the bisection search method.
- 5: $t_1 \leftarrow t_1 + 1$.
- 6: **Until** $t_1 = t_1^{\max}$ **or**

$$\epsilon_1^{(t_1+1)} = \frac{|\text{obj}^{(t_1+1)}(\mathbf{v}, \mathbf{f}) - \text{obj}^{(t_1)}(\mathbf{v}, \mathbf{f})|}{\text{obj}^{(t_1+1)}(\mathbf{v}, \mathbf{f})} < \epsilon.$$

of $(\mu_l, \mu_u) = (0, \min_k \frac{\xi_k v_k}{f_k^e})$. As $\sum_{k=1}^K f_k^e$ monotonically decreases w.r.t. μ , the optimal solution for f_k^e can be obtained by performing the bisection search based on (19). The algorithm for solving Problem $\mathcal{P}1$ is outlined in Algorithm 1. The complexity of Algorithm 1 is mainly dependent on the bisection search method. Given the convergence criterion ϵ and the maximum iteration time for variables $\{\mathbf{v}, \mathbf{f}\}$, denoted by t_1^{\max} , the overall complexity of Algorithm 1 can be expressed as $\mathcal{O}(t_1^{\max} \log_2(\frac{\mu_u - \mu_l}{\epsilon}) K)$.

B. Joint Optimization of Passive and Active Beamforming $\{\mathbf{F}_c, \mathbf{W}_c, \mathbf{w}_s, \boldsymbol{\theta}\}$

1) *Problem Reformulation:* With the optimized offloading volume \mathbf{v} , minimizing T_k is equivalent to minimizing the computing offloading latency. Therefore, given $\{\mathbf{v}, \mathbf{f}\}$, Problem $\mathcal{P}0$ is transformed into

$$\mathcal{P}2 : \min_{\mathbf{F}_c, \mathbf{W}_c, \mathbf{w}_s, \boldsymbol{\theta}} \sum_{k=1}^K \xi_k \frac{v_k}{R_k(\mathbf{F}_c, \mathbf{W}_{c,k}, \boldsymbol{\theta})} \quad (22)$$

s.t. (12b), (12c), (12d).

The OF of Problem $\mathcal{P}2$ is in a non-convex sum-of-ratios form, thereby presenting challenges in deriving solutions through the existing methods [34]. To address this issue, we first reformulate Problem $\mathcal{P}2$ by introducing an auxiliary variable $\boldsymbol{\lambda} = [\lambda_1, \dots, \lambda_K]$ as

$$\mathcal{P}2-1 : \min_{\mathbf{F}_c, \mathbf{W}_c, \mathbf{w}_s, \boldsymbol{\theta}, \boldsymbol{\lambda}} \sum_{k=1}^K \lambda_k$$

s.t. $\frac{\xi_k v_k}{R_k(\mathbf{F}_c, \mathbf{W}_{c,k}, \boldsymbol{\theta})} \leq \lambda_k, \forall k \in \mathcal{K},$ (23)

(12b), (12c), (12d).

Then, we introduce the following proposition for further derivation.

Proposition 1. If $\{\mathbf{F}_c^*, \mathbf{W}_c^*, \mathbf{w}_s^*, \boldsymbol{\theta}^*, \boldsymbol{\lambda}^*\}$ is the solution of Problem $\mathcal{P}2-1$, then $\boldsymbol{\delta}^* = [\delta_1, \dots, \delta_K]$ exists such that

$\{\mathbf{F}_c^*, \mathbf{W}_c^*, \mathbf{w}_s^*, \boldsymbol{\theta}^*\}$ satisfies the KKT conditions of the following problem when $\boldsymbol{\lambda} = \boldsymbol{\lambda}^*$ and $\boldsymbol{\delta} = \boldsymbol{\delta}^*$

$$\mathcal{P}2-2 : \min_{\mathbf{F}_c, \mathbf{W}_c, \mathbf{w}_s, \boldsymbol{\theta}} \sum_{k=1}^K \delta_k [\xi_k v_k - \lambda_k R_k(\mathbf{F}_c, \mathbf{W}_{c,k}, \boldsymbol{\theta})] \quad (24)$$

s.t. (12b), (12c), (12d).

Furthermore, $\{\mathbf{F}_c^*, \mathbf{W}_c^*, \boldsymbol{\theta}^*\}$ satisfies the following equations when $\boldsymbol{\lambda} = \boldsymbol{\lambda}^*$ and $\boldsymbol{\delta} = \boldsymbol{\delta}^*$

$$\begin{cases} \delta_k^* = \frac{1}{R_k(\mathbf{F}_c^*, \mathbf{W}_{c,k}^*, \boldsymbol{\theta}^*)}, \forall k \in \mathcal{K}, \\ \lambda_k^* = \frac{\xi_k v_k}{R_k(\mathbf{F}_c^*, \mathbf{W}_{c,k}^*, \boldsymbol{\theta}^*)}, \forall k \in \mathcal{K}. \end{cases} \quad (25)$$

Proof. Please refer to Appendix A. □

From Proposition 1, if $(\mathbf{F}_c^*, \mathbf{W}_c^*, \mathbf{w}_s^*, \boldsymbol{\theta}^*)$ is the solution to Problem $\mathcal{P}2-2$, and the value of $\boldsymbol{\lambda}$ and $\boldsymbol{\delta}$ are set following (25), then $(\mathbf{F}_c^*, \mathbf{W}_c^*, \mathbf{w}_s^*, \boldsymbol{\theta}^*, \boldsymbol{\lambda}^*)$ is the solution to Problem $\mathcal{P}2-1$. In the following, we propose an algorithm to solve Problem $\mathcal{P}2-3$ by alternately optimizing the sets $\{\boldsymbol{\lambda}, \boldsymbol{\delta}\}$ and $\{\mathbf{F}_c, \mathbf{W}_c, \mathbf{w}_s, \boldsymbol{\theta}\}$. Firstly, given $\{\mathbf{F}_c, \mathbf{W}_c, \mathbf{w}_s, \boldsymbol{\theta}\}$, $\boldsymbol{\lambda}$ and $\boldsymbol{\delta}$ are updated by using the modified Newton's method [22], [35]. Then, we optimize $\mathbf{F}_c, \mathbf{W}_c, \mathbf{w}_s$, and $\boldsymbol{\theta}$ given $\{\boldsymbol{\lambda}, \boldsymbol{\delta}\}$ according to Algorithm 3, which is discussed in the subsequent subsections. The procedure for solving Problem $\mathcal{P}2-2$ is summarized in Algorithm 2, where we have

$$\chi_k(\delta_k) = \delta_k R_k(\mathbf{F}_c^*, \mathbf{W}_{c,k}^*, \boldsymbol{\theta}^*) - 1, \forall k \in \mathcal{K}, \quad (26)$$

$$\kappa_k(\lambda_k) = \lambda_k R_k(\mathbf{F}_c^*, \mathbf{W}_{c,k}^*, \boldsymbol{\theta}^*) - \xi_k v_k, \forall k \in \mathcal{K}. \quad (27)$$

Algorithm 2 Joint optimization of $\{\mathbf{F}_c, \mathbf{W}_c, \mathbf{w}_s, \boldsymbol{\theta}\}$, given $\{\mathbf{v}, \mathbf{f}\}$.

- 1: Initialize iteration number $t_2 = 0$ and step $\zeta \in (0, 1)$. Set the maximum number of iterations to t_2^{\max} . Calculate $R_k^{(0)}$ using (35), $\boldsymbol{\delta}^{(0)}$ and $\boldsymbol{\lambda}^{(0)}$ using (25).
- 2: **Repeat**
- 3: Calculate $\{\mathbf{F}_c^{(t_2+1)}, \mathbf{W}_c^{(t_2+1)}, \mathbf{w}_s^{(t_2+1)}, \boldsymbol{\theta}^{(t_2+1)}\}$ using Algorithm 3.
- 4: Update $\delta_k^{(t_2+1)}$ and $\lambda_k^{(t_2+1)}$ by

$$\delta_k^{(t_2+1)} = \delta_k^{(t_2)} - \frac{\zeta^i \chi_k(\delta_k^{(t_2)})}{R_k^{(t_2+1)}(\mathbf{F}_c, \mathbf{W}_c, \boldsymbol{\theta})}, \quad (28)$$

$$\lambda_k^{(t_2+1)} = \lambda_k^{(t_2)} - \frac{\zeta^i \kappa_k(\lambda_k^{(t_2)})}{R_k^{(t_2+1)}(\mathbf{F}_c, \mathbf{W}_c, \boldsymbol{\theta})}, \quad (29)$$

where $i^{(t_2+1)}$ is the smallest integer satisfying

$$\begin{aligned} & \sum_{k=1}^K \left| \chi_k \left(\delta_k^{(t_2)} - \frac{\zeta^i \chi_k(\delta_k^{(t_2)})}{R_k^{(t_2+1)}(\mathbf{F}_c, \mathbf{W}_c, \boldsymbol{\theta})} \right) \right|^2 + \\ & \sum_{k=1}^K \left| \kappa_k \left(\lambda_k^{(t_2)} - \frac{\zeta^i \kappa_k(\lambda_k^{(t_2)})}{R_k^{(t_2+1)}(\mathbf{F}_c, \mathbf{W}_c, \boldsymbol{\theta})} \right) \right|^2 \\ & \leq (1 - \epsilon_3 \zeta^i)^2 \sum_{k=1}^K \left[\left| \chi_k(\delta_k^{(t_2+1)}) \right|^2 + \left| \kappa_k(\lambda_k^{(t_2+1)}) \right|^2 \right]. \end{aligned} \quad (30)$$

- 5: $t_2 \leftarrow t_2 + 1$.

- 6: **Until** $\chi_k(\delta_k^{(t_2)}) = 0$ and $\kappa_k(\lambda_k^{(t_2)}) = 0$ **or** $t_2 = t_2^{\max}$.
-

2) *Joint Active and Passive Beamforming Optimization:* In this case, Problem $\mathcal{P}2$ -2 can be transformed into

$$\mathcal{P}2\text{-3} : \max_{\mathbf{F}_c, \mathbf{W}_c, \mathbf{w}_s, \boldsymbol{\theta}} \sum_{k=1}^K \delta_k \lambda_k R_k(\mathbf{F}_c, \mathbf{W}_{c,k}, \boldsymbol{\theta}) \quad (31)$$

$$s.t. \quad (12b), (12c), (12d).$$

a) *OF Reformulation and Decoding Matrix Design:* By introducing an auxiliary matrix \mathbf{D}_k , the equivalent formulation of Problem $\mathcal{P}2$ -3 with constants removed can be derived as [36]

$$\mathcal{P}2\text{-4} : \min_{\mathbf{F}_c, \mathbf{W}_c, \mathbf{w}_s, \boldsymbol{\theta}, \mathbf{D}} \sum_{k=1}^K \delta_k \lambda_k \text{Tr}(\mathbf{D}_k \mathbf{E}_k(\mathbf{F}_c, \mathbf{W}_{c,k}, \boldsymbol{\theta})) - \delta_k \lambda_k \log_2 |\mathbf{D}_k| \quad (32)$$

$$s.t. \quad (12b), (12c), (12d),$$

where $\mathbf{D} = \{\mathbf{D}_k, \forall k \in \mathcal{K}\}$ and $\mathbf{E}_k(\mathbf{F}_c, \mathbf{W}_{c,k}, \boldsymbol{\theta}) \in \mathbb{C}^{d \times d}$ is the mean-square error (MSE) matrix of UE k given by

$$\begin{aligned} \mathbf{E}_k(\mathbf{F}_c, \mathbf{W}_{c,k}, \boldsymbol{\theta}) &= \mathbb{E}[(\hat{\mathbf{c}}_k - \mathbf{c}_k)(\hat{\mathbf{c}}_k - \mathbf{c}_k)^H] \\ &= (\mathbf{W}_{c,k}^H \mathbf{H}_k \mathbf{F}_{c,k} - \mathbf{I})(\mathbf{W}_{c,k}^H \mathbf{H}_k \mathbf{F}_{c,k} - \mathbf{I})^H \\ &+ \sum_{i=1, i \neq k}^K \mathbf{W}_{c,k}^H \mathbf{H}_i \mathbf{F}_{c,i} \mathbf{F}_{c,i}^H \mathbf{H}_i^H \mathbf{W}_{c,k} + \sigma_c^2 \mathbf{W}_{c,k}^H \mathbf{W}_{c,k}. \end{aligned}$$

In the following, we design an algorithm for solving Problem $\mathcal{P}2$ -4 by alternately optimizing the beamforming variables $\{\mathbf{F}_c, \mathbf{W}_c, \mathbf{w}_s, \boldsymbol{\theta}\}$ under the BCD framework. Given $\{\mathbf{F}_c, \mathbf{w}_s, \boldsymbol{\theta}\}$, Problem $\mathcal{P}2$ -4 is marginal convex w.r.t. $\{\mathbf{W}_c, \mathbf{D}\}$. Hence, by setting the first-order derivative of the OF of Problem $\mathcal{P}2$ -4 w.r.t. $\mathbf{W}_{c,k}$ and \mathbf{D}_k to zero, respectively, the optimal solutions are obtained as

$$\mathbf{W}_{c,k}^* = (\mathbf{J}_k + \mathbf{H}_k \mathbf{F}_{c,k} \mathbf{F}_{c,k}^H \mathbf{H}_k^H)^{-1} \mathbf{H}_k \mathbf{F}_{c,k}, \quad (33)$$

$$\mathbf{D}_k^* = (\mathbf{E}_k^{(\text{MMSE})})^{-1}, \quad (34)$$

where

$$\mathbf{E}_k^{(\text{MMSE})} = \mathbf{I}_d - \mathbf{F}_{c,k}^H \mathbf{H}_k^H (\mathbf{J}_k + \mathbf{H}_k \mathbf{F}_{c,k} \mathbf{F}_{c,k}^H \mathbf{H}_k^H)^{-1} \mathbf{H}_k \mathbf{F}_{c,k}$$

is the minimum mean square error (MMSE) of UE k .

Meanwhile, R_k is given by

$$R_k = B_\omega \log_2 |(\mathbf{E}_k^{(\text{MMSE})})^{-1}|. \quad (35)$$

b) *Receive and Transmit Beamforming Design for the UE:* We first consider the optimization of the receive beamforming vector $\mathbf{w}_{s,k}$ of UE k with fixed \mathbf{F}_c . Note that $\mathbf{w}_{s,k}$ is only related to the radar SINR constraint (12c). The optimal $\mathbf{w}_{s,k}$ that maximizes the sensing SINR is given by

$$\mathbf{w}_{s,k}^* = \arg \max_{\mathbf{w}_{s,k}} \frac{\mathbf{w}_{s,k}^H \mathbf{G}_k \mathbf{F}_{c,k} \mathbf{F}_{c,k}^H \mathbf{G}_k^H \mathbf{w}_{s,k}}{\mathbf{w}_{s,k}^H \mathbf{T}_k \mathbf{w}_{s,k}}, \quad (36)$$

which equals the eigenvector corresponding to the largest generalized eigenvalue of the matrix $[\mathbf{T}_k^{-1} \mathbf{G}_k \mathbf{F}_{c,k} \mathbf{F}_{c,k}^H \mathbf{G}_k^H]$ according to the MVDR method [37].

In the following, we focus on optimizing the transmit beamforming matrices \mathbf{F}_c with the fixed $\mathbf{w}_{s,k}$. First, the non-convex fractional inequalities (12c) can be rewritten as

$$\eta \text{Tr}(\mathbf{T}_k \mathbf{w}_{s,k} \mathbf{w}_{s,k}^H) - \text{Tr}(\mathbf{G}_k \mathbf{F}_{c,k} \mathbf{F}_{c,k}^H \mathbf{G}_k^H \mathbf{w}_{s,k} \mathbf{w}_{s,k}^H) \leq 0, \forall k \in \mathcal{K}, \quad (37)$$

where the SCA method can be applied to derive a convex upper bound of (37). By defining $f(\mathbf{F}_c) \triangleq -\text{Tr}(\mathbf{G}_k \mathbf{F}_{c,k} \mathbf{F}_{c,k}^H \mathbf{G}_k^H \mathbf{w}_{s,k} \mathbf{w}_{s,k}^H)$, the first-order Taylor approximation of $f(\mathbf{F}_c)$ at $\mathbf{F}_c^{(t)}$ in the t -th iteration can be formulated as

$$\begin{aligned} f(\mathbf{F}_c, \mathbf{F}_c^{(t)}) &= \text{Tr}(\mathbf{G}_k^T \mathbf{w}_{s,k}^* \mathbf{w}_{s,k}^T \mathbf{G}_k^* \mathbf{F}_{c,k}^{(t)*} \mathbf{F}_{c,k}^{(t),T}) \\ &- 2 \text{Re}\{\text{Tr}(\mathbf{G}_k^H \mathbf{w}_{s,k} \mathbf{w}_{s,k}^H \mathbf{G}_k \mathbf{F}_{c,k} \mathbf{F}_{c,k}^{(t),H})\}. \end{aligned} \quad (38)$$

Then, with $\{\mathbf{W}_c, \mathbf{w}_s, \boldsymbol{\theta}, \mathbf{D}\}$ fixed, Problem $\mathcal{P}2$ -4 can be approximated as

$$\begin{aligned} \mathcal{P}2\text{-5} : \min_{\mathbf{F}_c} \sum_{k=1}^K \sum_{i=1}^K \delta_k \lambda_k \text{Tr}(\mathbf{D}_k \mathbf{W}_{c,k}^H \mathbf{H}_i \mathbf{F}_{c,i} \mathbf{F}_{c,i}^H \mathbf{H}_i^H \mathbf{W}_{c,k}) - \sum_{k=1}^K \delta_k \lambda_k \text{Tr}(\mathbf{D}_k (\mathbf{F}_{c,k}^H \mathbf{H}_k^H \mathbf{W}_{c,k} + \mathbf{W}_{c,k}^H \mathbf{H}_k \mathbf{F}_{c,k})) \\ s.t. \quad \text{Tr}(\mathbf{R}_{\mathbf{x},k}) \leq P_{t,k}, \forall k \in \mathcal{K}, \\ \eta \text{Tr}(\mathbf{T}_k \mathbf{w}_{s,k} \mathbf{w}_{s,k}^H) + f(\mathbf{F}_c, \mathbf{F}_c^{(t)}) \leq 0, \forall k \in \mathcal{K}. \end{aligned} \quad (39)$$

It can be verified that Problem $\mathcal{P}2$ -5 is a convex problem, which can be efficiently solved via CVX [38].

c) *RIS Phase Shift Design:* Finally, we focus on the optimization of the phase shift of the RIS $\boldsymbol{\theta}$. The corresponding subproblem can be formulated as

$$\begin{aligned} \mathcal{P}2\text{-6} : \min_{\boldsymbol{\theta}} \sum_{k=1}^K \sum_{i=1}^K \delta_k \lambda_k \text{Tr}(\mathbf{D}_k \mathbf{W}_{c,k}^H \mathbf{H}_i \mathbf{F}_{c,i} \mathbf{F}_{c,i}^H \mathbf{H}_i^H \mathbf{W}_{c,k}) - \sum_{k=1}^K \delta_k \lambda_k \text{Tr}(\mathbf{D}_k (\mathbf{F}_{c,k}^H \mathbf{H}_k^H \mathbf{W}_{c,k} + \mathbf{W}_{c,k}^H \mathbf{H}_k \mathbf{F}_{c,k})) \\ s.t. \quad 0 < \theta_l \leq 2\pi, \forall l \in \mathcal{L}. \end{aligned} \quad (40)$$

By defining $\mathbf{H}_k \triangleq \mathbf{H}_{\text{bu},k} + \mathbf{H}_r \mathbf{V} \mathbf{H}_{\text{ru},k}$, we have

$$\begin{aligned} \mathbf{D}_k \mathbf{W}_{c,k}^H \mathbf{H}_i \mathbf{F}_{c,i} \mathbf{F}_{c,i}^H \mathbf{H}_i^H \mathbf{W}_{c,k} &= \mathbf{D}_k \mathbf{W}_{c,k}^H \mathbf{H}_{\text{bu},i} \mathbf{F}_{c,i} \mathbf{F}_{c,i}^H \mathbf{H}_{\text{ru},i}^H \mathbf{V}^H \mathbf{H}_r^H \mathbf{W}_{c,k} \\ &+ \mathbf{D}_k \mathbf{W}_{c,k}^H \mathbf{H}_r \mathbf{V} \mathbf{H}_{\text{ru},i} \mathbf{F}_{c,i} \mathbf{F}_{c,i}^H \mathbf{H}_{\text{bu},i}^H \mathbf{W}_{c,k} \\ &+ \mathbf{D}_k \mathbf{W}_{c,k}^H \mathbf{H}_r \mathbf{V} \mathbf{H}_{\text{ru},i} \mathbf{F}_{c,i} \mathbf{F}_{c,i}^H \mathbf{H}_{\text{ru},i}^H \mathbf{V}^H \mathbf{H}_r^H \mathbf{W}_{c,k} \\ &+ \mathbf{D}_k \mathbf{W}_{c,k}^H \mathbf{H}_{\text{bu},i} \mathbf{F}_{c,i} \mathbf{F}_{c,i}^H \mathbf{H}_{\text{bu},i}^H \mathbf{W}_{c,k}, \end{aligned} \quad (41)$$

and

$$\begin{aligned} \mathbf{D}_k (\mathbf{F}_{c,k}^H \mathbf{H}_k^H \mathbf{W}_{c,k} + \mathbf{W}_{c,k}^H \mathbf{H}_k \mathbf{F}_{c,k}) &= \mathbf{D}_k \mathbf{F}_{c,k}^H \mathbf{H}_{\text{ru},k}^H \mathbf{V}^H \mathbf{H}_r^H \mathbf{W}_{c,k} + \mathbf{D}_k \mathbf{F}_{c,k}^H \mathbf{H}_{\text{bu},k}^H \mathbf{W}_{c,k} \\ &+ \mathbf{D}_k \mathbf{W}_{c,k}^H \mathbf{H}_r \mathbf{V} \mathbf{H}_{\text{ru},k} \mathbf{F}_{c,k} + \mathbf{D}_k \mathbf{W}_{c,k}^H \mathbf{H}_{\text{bu},k} \mathbf{F}_{c,k}. \end{aligned} \quad (42)$$

By defining $\mathbf{S}_{k,i} \triangleq \mathbf{H}_r^H \mathbf{W}_{c,k} \mathbf{D}_k \mathbf{W}_{c,k}^H \mathbf{H}_{\text{bu},i} \mathbf{F}_{c,i} \mathbf{F}_{c,i}^H \mathbf{H}_{\text{ru},i}^H$, $\mathbf{B}_i \triangleq \mathbf{H}_{\text{ru},i} \mathbf{F}_{c,i} \mathbf{F}_{c,i}^H \mathbf{H}_{\text{ru},i}^H$, $\mathbf{C}_k \triangleq \mathbf{H}_r^H \mathbf{W}_{c,k} \mathbf{D}_k \mathbf{W}_{c,k}^H \mathbf{H}_r$, and $\mathbf{P}_{k,i} \triangleq \mathbf{H}_{\text{ru},i} \mathbf{F}_{c,i} \mathbf{D}_k \mathbf{W}_{c,k}^H \mathbf{H}_r$, (41) and (42) are further transformed to

$$\begin{aligned} \text{Tr}(\mathbf{D}_k \mathbf{W}_{c,k}^H \mathbf{H}_i \mathbf{F}_{c,i} \mathbf{F}_{c,i}^H \mathbf{H}_i^H \mathbf{W}_{c,k}) &= \text{Tr}(\mathbf{V} \mathbf{B}_i \mathbf{V}^H \mathbf{C}_k) + \text{Tr}(\mathbf{V}^H \mathbf{S}_{k,i}) + \text{Tr}(\mathbf{V} \mathbf{S}_{k,i}^H) + \text{const}_1, \end{aligned} \quad (43)$$

and

$$\begin{aligned} \text{Tr}(\mathbf{D}_k (\mathbf{F}_{c,k}^H \mathbf{H}_k^H \mathbf{W}_{c,k} + \mathbf{W}_{c,k}^H \mathbf{H}_k \mathbf{F}_{c,k})) &= \text{Tr}(\mathbf{P}_{k,i} \mathbf{V}) + \text{Tr}(\mathbf{P}_{k,i}^H \mathbf{V}^H) + \text{const}_2, \end{aligned} \quad (44)$$

where const_1 and const_2 are constant independent of \mathbf{V} . Thus, Problem $\mathcal{P}2$ -6 can be rewritten as

$$\mathcal{P}2\text{-7} : \min_{\boldsymbol{\theta}} \text{Tr}(\mathbf{V} \mathbf{B} \mathbf{V}^H \mathbf{C}) + \text{Tr}(\mathbf{V} \mathbf{U}) + \text{Tr}(\mathbf{V}^H \mathbf{U}^H) \quad (45)$$

$$s.t. \quad 0 < \theta_l \leq 2\pi, \forall l \in \mathcal{L},$$

where $\mathbf{B} \triangleq \sum_{i=1}^K \mathbf{B}_i$, $\mathbf{C} \triangleq \sum_{k=1}^K \delta_k \lambda_k \mathbf{C}_k$, and $\mathbf{U} \triangleq \sum_{i=1}^K \sum_{k=1}^K \delta_k \lambda_k (\mathbf{S}_{k,i}^H - \mathbf{P}_{k,i})$.

With the definitions of $\phi \triangleq [e^{j\theta_1}, \dots, e^{j\theta_L}]^T$ and $\mathbf{u} = [[\mathbf{U}]_{1,1}, \dots, [\mathbf{U}]_{L,L}]^T$, we have

$$\text{Tr}(\mathbf{V}\mathbf{B}\mathbf{V}^H\mathbf{C}) = \phi^H(\mathbf{C} \odot \mathbf{B}^T)\phi, \quad (46)$$

and

$$\text{Tr}(\mathbf{V}\mathbf{U}) = \phi^T \mathbf{u}, \text{Tr}(\mathbf{V}^H \mathbf{U}^H) = \mathbf{u}^H \phi^*. \quad (47)$$

Accordingly, Problem $\mathcal{P}2-7$ can be reformulated as

$$\begin{aligned} \mathcal{P}2-8 : \min_{\phi} \quad & g(\phi) = \phi^H \Xi \phi + 2\text{Re}\{\phi^H \mathbf{u}^*\} \\ s.t. \quad & |\phi_l| = 1, \forall l \in \mathcal{L}, \end{aligned} \quad (48)$$

where $\Xi \triangleq \mathbf{C} \odot \mathbf{B}^T$. Problem $\mathcal{P}2-8$ is a non-convex problem owing to the unit modulus constraint. In the following, the MM algorithm [39] with two steps is applied to tackle this problem. Specifically, the surrogate function $h(\phi|\phi^{(t)})$ at the t -th iteration $\phi^{(t)}$, is introduced in the majorization step to provide an upper bound for $g(\phi)$. Then, in the minimization step, we update ϕ by $\phi^{(t+1)} \in \arg \min_{\phi} h(\phi|\phi^{(t)})$. To this end, we introduce the lemma below to construct the surrogate function of $g(\phi)$.

Lemma 1. *By denoting the maximum eigenvalue of Ξ by λ_{\max} , we have*

$$\begin{aligned} g(\phi) &\leq \phi^H \lambda_{\max} \mathbf{I}_L \phi - 2\text{Re}\{\phi^H (\lambda_{\max} \mathbf{I}_L - \Xi) \phi^{(t)}\} \\ &+ \phi^{(t)H} (\lambda_{\max} \mathbf{I}_L - \Xi) \phi^{(t)} + 2\text{Re}\{\phi^H \mathbf{u}^*\} \triangleq h(\phi|\phi^{(t)}). \end{aligned} \quad (49)$$

Proof. Please refer to [39], [40]. \square

Note that $\phi^H \phi = L$, $\phi^H \lambda_{\max} \mathbf{I}_L \phi = L \lambda_{\max}$ is a constant. Thus, with constants independent of ϕ removed, Problem $\mathcal{P}2-8$ with the surrogate function at the $t+1$ -th iteration can be formulated as

$$\begin{aligned} \mathcal{P}2-9 : \max_{\phi} \quad & \text{Re}\{\phi^H [(\lambda_{\max} \mathbf{I}_L - \Xi) \phi^{(t)} - \mathbf{u}^*]\} \\ s.t. \quad & |\phi_l| = 1, \forall l \in \mathcal{L}. \end{aligned} \quad (50)$$

Thus, the optimal solution for θ at the $(t+1)$ -th iteration is given by

$$\theta^{(t+1)} = \angle((\lambda_{\max} \mathbf{I}_L - \Xi) \phi^{(t)} - \mathbf{u}^*). \quad (51)$$

According to the preceding analysis, the procedure for solving Problem $\mathcal{P}2-4$ is summarized in Algorithm 3. The complexity of this algorithm is provided as follows. Since the number of variables in Step 3 is KNd , the complexity of updating $\mathbf{F}_c^{(t_3+1)}$ via the SCA method is given by $\mathcal{O}((KNd)^{3.5})$. In Step 4, the complexities of calculating $\mathbf{W}_c^{(t_3+1)}$ and $\mathbf{D}^{(t_3+1)}$ are on the order of $\mathcal{O}(KM^3)$ and $\mathcal{O}(Kd^3)$, respectively. In Step 5, the complexity of calculating $\mathbf{w}_s^{(t_3+1)}$ is $\mathcal{O}(KN^3)$. Defining the number of iterations as t_{MM}^{\max} , the computation complexity of updating $\theta^{(t_3+1)}$ via the MM algorithm in Step 6 contains two parts. Specifically, the complexity of calculating the maximum eigenvalue λ_{\max} of Ξ is on the order of $\mathcal{O}(L^3)$. Note that the main complexity

Algorithm 3 Joint optimization of $\{\mathbf{F}_c, \mathbf{W}_c, \mathbf{w}_s, \theta\}$, Given $\{\delta, \lambda\}$.

- 1: Initialize iteration number $t_3 = 0$. Set the maximum number of iterations to t_3^{\max} . Initialize feasible $\mathbf{F}_c^{(0)}$, $\mathbf{w}_s^{(0)}$ and $\theta^{(0)}$ following constraints (12b) - (12d). Calculate $R_k^{(0)}$ using (35).
- 2: **Repeat**
- 3: Update $\mathbf{F}_c^{(t_3+1)}$ by solving Problem 2-5 with the SCA method.
- 4: Calculate $\mathbf{W}_c^{(t_3+1)}$ and $\mathbf{D}^{(t_3+1)}$ according to (33) and (34), respectively.
- 5: Calculate $\mathbf{w}_s^{(t_3+1)}$ by using (36).
- 6: Update $\theta^{(t_3+1)}$ using MM algorithm.
- 7: $t_3 \leftarrow t_3 + 1$.
- 8: **Until** $t_3 = t_3^{\max}$ **or**

$$\epsilon_3^{(t_3+1)} = \frac{|\text{obj}^{(t_3+1)}(\mathbf{F}_c, \theta) - \text{obj}^{(t_3)}(\mathbf{F}_c, \theta)|}{\text{obj}^{(t_3+1)}(\mathbf{F}_c, \theta)} < \epsilon.$$

for each iteration of the MM algorithm arises from calculating $\phi^{(t)}$, whose complexity is given by $\mathcal{O}(L^2)$. Hence, the total complexity of updating $\theta^{(t_3+1)}$ is on the order of $\mathcal{O}(L^3 + t_{MM}^{\max} L^2)$. By aggregating these components, the overall complexity of Algorithm 3 is given by $\mathcal{O}(t_3^{\max} \cdot \max\{(KNd)^{3.5}, KM^3, Kd^3, KN^3, L^3 + t_{MM}^{\max} L^2\})$. Furthermore, the complexity of Algorithm 2 is dominated by calculating $\{\mathbf{F}_c^{(t_2+1)}, \mathbf{W}_c^{(t_2+1)}, \mathbf{w}_s^{(t_2+1)}, \theta^{(t_2+1)}\}$ using Algorithm 3, as all other steps involve explicit closed-form solutions.

C. Summarize of the Algorithm Development

Following the above discussions, we present the overall BCD algorithm for solving Problem $\mathcal{P}0$ in Algorithm 4. The monotonic increase in the OF value of Problem $\mathcal{P}0$ at each step of Algorithm 4 is readily verified. Furthermore, the edge computing resource constraints impose an upper bound on the OF value. Hence, Algorithm 4 is guaranteed to converge. The complexity of Algorithm 4 is mainly determined by Step 3 and Step 4, the complexities of which have been thoroughly discussed in the preceding subsections.

Algorithm 4 Joint optimization of $\mathbf{v}, \mathbf{f}, \mathbf{F}_c$ and θ .

- 1: Initialize iteration number $t_4 = 0$. Set the maximum number of iterations to t_4^{\max} . Initialize feasible $\mathbf{f}^{(0)}$, $\mathbf{F}_c^{(0)}$, $\mathbf{w}_s^{(0)}$ and $\theta^{(0)}$ following constraints (12b) - (12e) and (12g).
- 2: **Repeat**
- 3: Calculate $\mathbf{v}^{(t_4+1)}$ and $\mathbf{f}^{(t_4+1)}$ via Algorithm 1.
- 4: Calculate $\mathbf{F}_c^{(t_4+1)}$, $\mathbf{W}_c^{(t_4+1)}$, $\mathbf{w}_s^{(t_4+1)}$ and $\theta^{(t_4+1)}$ via Algorithm 2.
- 5: $t_4 \leftarrow t_4 + 1$.
- 6: **Until** $t_4 = t_4^{\max}$ **or**

$$\epsilon_4^{(t_4+1)} = \frac{|\text{obj}^{(t_4+1)}(\mathbf{v}, \mathbf{f}, \mathbf{F}_c, \theta) - \text{obj}^{(t_4)}(\mathbf{v}, \mathbf{f}, \mathbf{F}_c, \theta)|}{\text{obj}^{(t_4+1)}(\mathbf{v}, \mathbf{f}, \mathbf{F}_c, \theta)} < \epsilon.$$

IV. SPECIFIC CASE STUDY

A special case with a single UE that transmits a single data stream is studied in this section to provide a comprehensive characterization of the RIS-assisted ICSC system. Since the number of the data streams d is assumed to be 1, the radar SINR constraint (12c) degenerates to the SNR constraint. Furthermore, as there is no need for the consideration of edge computing resource allocation, the sum-of-ratios form in the OF of Problem $\mathcal{P}2$ is transformed into a single-ratio form. In this instance, Problem $\mathcal{P}0$ is simplified as follows:

$$\mathcal{P}3: \min_{\mathbf{f}_c, \mathbf{w}_c, \mathbf{w}_s, \theta, v} T(\mathbf{f}_c, \mathbf{w}_c, \theta, v) \quad (52a)$$

$$s.t. \quad \text{Tr}(\mathbf{R}_X) \leq P_t, \quad (52b)$$

$$\gamma \geq \eta, \quad (52c)$$

$$0 < \theta_l \leq 2\pi, \forall l \in \mathcal{L}, \quad (52d)$$

$$v \in \{0, 1, \dots, V\}. \quad (52e)$$

where η represents the SNR threshold of the UE for radar sensing, $\mathbf{f}_c \in \mathbb{C}^{N \times 1}$ and $\mathbf{w}_c \in \mathbb{C}^{M \times 1}$ denote the precoding and decoding vectors, respectively.

The BCD method is employed to solve Problem $\mathcal{P}3$. As discussed in Sec. III-A, given $\{\mathbf{f}_c, \mathbf{w}_c, \mathbf{w}_s, \theta\}$, the optimal solution for v is obtained when $T_1 = T_c$. Consequently, the optimal v is equal to

$$v^* = \arg \min_{\hat{v} \in \{\lceil \hat{v}^* \rceil, \lfloor \hat{v}^* \rfloor\}} T(\hat{v}), \quad (53)$$

where

$$\hat{v}^* = \frac{VcRf_{\text{total}}^e}{f_{\text{total}}^e f^l + cR(f_{\text{total}}^e + f^l)}. \quad (54)$$

Given v , Problem $\mathcal{P}3$ can be rewritten as

$$\mathcal{P}3-1: \max_{\mathbf{f}_c, \mathbf{w}_c, \mathbf{w}_s, \theta} R(\mathbf{f}_c, \mathbf{w}_c, \theta) \quad (55)$$

$$s.t. \quad (52b), (52c), (52d).$$

Since $R(\mathbf{f}_c, \mathbf{w}_c, \theta)$ monotonically increases w.r.t. $\frac{|\mathbf{w}_c^H \mathbf{H} \mathbf{f}_c|^2}{\sigma_c^2 \|\mathbf{w}_c^H\|^2}$, Problem $\mathcal{P}3-1$ is equivalent to

$$\mathcal{P}3-2: \max_{\mathbf{f}_c, \mathbf{w}_c, \mathbf{w}_s, \theta} \frac{|\mathbf{w}_c^H \mathbf{H} \mathbf{f}_c|^2}{\sigma_c^2 \|\mathbf{w}_c^H\|^2} \quad (56)$$

$$s.t. \quad (52b), (52c), (52d).$$

Note that \mathbf{w}_s is only related to constraint (52c), while \mathbf{w}_c is related to the OF of Problem $\mathcal{P}3-2$. Therefore, the optimal solution for the decoding matrices \mathbf{w}_s and \mathbf{w}_c can be derived based on the maximum ratio combining (MRC) criterion as

$$\mathbf{w}_s^* = \arg \max \left(\frac{|\mathbf{w}_s^H \mathbf{G} \mathbf{f}_c|^2}{\|\mathbf{w}_s^H\|^2} \right) = \mathbf{G} \mathbf{f}_c, \quad (57)$$

$$\mathbf{w}_c^* = \arg \max \left(\frac{|\mathbf{w}_c^H \mathbf{H} \mathbf{f}_c|^2}{\|\mathbf{w}_c^H\|^2} \right) = \mathbf{H} \mathbf{f}_c. \quad (58)$$

By defining $\mathbf{h} = \frac{\mathbf{H}^H \mathbf{w}_c}{\sigma_c \|\mathbf{w}_c^H\|} \in \mathbb{C}^{N \times 1}$ and $\mathbf{g} = \frac{\mathbf{G}^H \mathbf{w}_s}{\sigma_s \|\mathbf{w}_s^H\|} \in \mathbb{C}^{N \times 1}$, the subproblem of optimizing \mathbf{f}_c can be formulated as follows:

$$\mathcal{P}3-3: \max_{\mathbf{f}_c} \left| \mathbf{h}^H \mathbf{f}_c \right|^2 \quad (59a)$$

$$s.t. \quad \|\mathbf{f}_c\|^2 \leq P_t, \quad (59b)$$

$$\left| \mathbf{g}^H \mathbf{f}_c \right|^2 \geq \eta. \quad (59c)$$

The following proposition contributes to addressing Problem $\mathcal{P}3-3$ [41], [42].

Proposition 2. *The optimal solution to Problem $\mathcal{P}3-3$ can be expressed as*

$$\mathbf{f}_c = a\mathbf{h} + b\mathbf{g}, \quad (60)$$

where $a, b \in \mathbb{C}$ are given as follows:

Case 1: If $\eta \leq \frac{P_t \|\mathbf{g}^H \mathbf{h}\|^2}{\|\mathbf{h}\|^2}$,

$$\begin{cases} |a| = \frac{\sqrt{P_t}}{\|\mathbf{h}\|}, \\ |b| = 0, \end{cases} \quad (61)$$

with an arbitrary phase shift.

Case 2: If $\frac{P_t \|\mathbf{g}^H \mathbf{h}\|^2}{\|\mathbf{h}\|^2} \leq \eta \leq P_t \|\mathbf{g}\|^2$,

$$\begin{cases} |a| = \sqrt{\frac{P_t \|\mathbf{g}\|^2 - \eta}{\|\mathbf{h}\|^2 \|\mathbf{g}\|^2 - |\mathbf{h}^H \mathbf{g}|^2}}, \\ |b| = \frac{\sqrt{\eta}}{\|\mathbf{g}\|^2} - \frac{|\mathbf{h}^H \mathbf{g}|}{\|\mathbf{g}\|^2} |a|, \end{cases} \quad (62)$$

where the phase of a and b should satisfy

$$\angle(a) - \angle(b) = \angle(\mathbf{h}^H \mathbf{g}). \quad (63)$$

Case 3: If $\eta > P_t \|\mathbf{g}\|^2$, there exists no feasible solution.

Proof. Please refer to Appendix B. \square

Given $\{v, \mathbf{f}_c, \mathbf{w}_s, \mathbf{w}_c\}$, the following inequality holds for the OF of Problem $\mathcal{P}3-2$.

$$\frac{|\mathbf{w}_c^H (\mathbf{H}_{bu} + \mathbf{H}_r \mathbf{V} \mathbf{H}_{ru}) \mathbf{f}_c|^2}{\sigma_c^2 \|\mathbf{w}_c^H\|^2} \leq \frac{|\mathbf{w}_c^H \mathbf{H}_{bu} \mathbf{f}_c|^2}{\sigma_c^2 \|\mathbf{w}_c^H\|^2} + \frac{|\mathbf{w}_c^H \mathbf{H}_r \mathbf{V} \mathbf{H}_{ru} \mathbf{f}_c|^2}{\sigma_c^2 \|\mathbf{w}_c^H\|^2}. \quad (64)$$

Therefore, the optimal solution of θ can be obtained via the following equation

$$\theta = \angle(\mathbf{w}_c^H \mathbf{H}_{bu} \mathbf{f}_c) - \angle(\text{diag}\{\mathbf{w}_c^H \mathbf{H}_r\} \mathbf{H}_{ru} \mathbf{f}_c). \quad (65)$$

The overall algorithm for Problem $\mathcal{P}3$ is summarized in Algorithm 5. Next, we analyze the complexity of this algorithm. Note that the complexity of Algorithm 5 is dominated by Steps 4-6. Firstly, the complexities of using the MRC criterion to calculate $\mathbf{w}_c^{(t_5+1)}$ and $\mathbf{w}_s^{(t_5+1)}$ are on the order of $\mathcal{O}(N^2)$ and $\mathcal{O}(MN)$, respectively. Secondly, the complexity of calculating $\mathbf{f}_c^{(t_5+1)}$ following Proposition 2 is given by $\mathcal{O}(\max\{MN, N^2\})$. Finally, the complexity of calculating $\theta^{(t_5+1)}$ by using (65) is $\mathcal{O}(L^2N)$. Considering that $L \gg \{M, N\}$, the complexity of Algorithm 5 is on the order of $\mathcal{O}(L^2N)$.

Algorithm 5 Joint optimization of v , \mathbf{w}_c , \mathbf{w}_s , \mathbf{f}_c and $\boldsymbol{\theta}$

- 1: Initialize iteration number $t_5 = 0$. Set the maximum number of iterations to t_5^{\max} . Initialize feasible $\mathbf{f}_c^{(0)}$, $\mathbf{w}_c^{(0)}$, $\mathbf{w}_s^{(0)}$ and $\boldsymbol{\theta}^{(0)}$ following constraints (52b) - (52e).
- 2: **Repeat**
- 3: Calculate v by using (54)
- 4: Calculate $\mathbf{w}_c^{(t_5+1)}$ and $\mathbf{w}_s^{(t_5+1)}$ by using (57) and (58), respectively.
- 5: Calculate $\mathbf{f}_c^{(t_5+1)}$ following Proposition 2.
- 6: Calculate $\boldsymbol{\theta}^{(t_5+1)}$ by using (65).
- 7: $t_5 \leftarrow t_5 + 1$.
- 8: **Until** $t_5 = t_5^{\max}$ **or**

$$\epsilon_5^{(t_5+1)} = \frac{\left| \text{obj}^{(t_5+1)}(v, \mathbf{w}_c, \mathbf{f}_c, \boldsymbol{\theta}) - \text{obj}^{(t_5)}(v, \mathbf{w}_c, \mathbf{f}_c, \boldsymbol{\theta}) \right|}{\text{obj}^{(t_5+1)}(v, \mathbf{w}_c, \mathbf{f}_c, \boldsymbol{\theta})} < \epsilon.$$

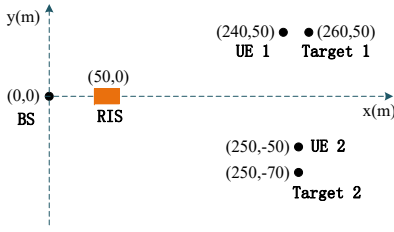


Fig. 2. The simulated multi-UE RIS-assisted ICSC scenario

V. SIMULATION RESULTS

In this section, numerical results are provided to validate the performance of the proposed RIS-assisted ICSC system in both single-UE and multi-UE scenarios. As shown in Fig. 2, the BS and the RIS are located at (0, 0) and (200 m, 0), respectively. In the multi-UE scenario, we assume that two UEs are located at (240 m, 50 m) and (250 m, -50 m), with corresponding targets at (260 m, 50 m) and (250 m, -70 m), respectively. For the single-UE scenario, the UE is located at (250 m, 50 m) with its target at (270 m, 50 m).

In the context of wireless communication channels, we account for both small-scale fading and large-scale path loss. In specific, the large-scale path loss in dB is expressed as

$$PL = PL_0 - 10\alpha \log_{10} \left(\frac{d}{d_0} \right), \quad (66)$$

where PL_0 is the path loss at the reference distance d_0 , d represents the link distance and α denotes the corresponding path loss exponent. The path loss exponent of the UE-BS link, UE-RIS link, RIS-BS link, and UE-UE interference channel are denoted by α_{bu} , α_{ru} , and α_r , α_{uu} , respectively. The Rayleigh channel model is employed to characterize the communication channels between the BS and UEs, as well as the channels between UEs, due to the presence of potential scatters and obstacles. While the small-scale fading of channels associated with the RIS is assumed to follow a Rician fading distribution:

$$\tilde{\mathbf{H}} = \sqrt{\frac{K_R}{1 + K_R}} \tilde{\mathbf{H}}_{\text{LoS}} + \sqrt{\frac{1}{1 + K_R}} \tilde{\mathbf{H}}_{\text{NLoS}}, \quad (67)$$

where K_R is the Rician factor, $\tilde{\mathbf{H}}_{\text{LoS}}$ denotes the line of sight (LoS) component, and $\tilde{\mathbf{H}}_{\text{NLoS}}$ represents the non-line of sight

TABLE I
DEFAULT SIMULATION PARAMETER SETTINGS

Description	Parameter and Value
Communication and Radar model	$PL_0 = 30$ dB, $d_0 = 1$ m
	$\alpha_{bu} = 3.75$, $\alpha_r = 2.2$, $\alpha_{ru} = 2.2$
	$\alpha_{uu} = 2.2$, $B_\omega = 1$ MHz
	$M = 4$, $N = 2$, $d = 2$
	$P_{t,k}^{\max} = 10$ mW, $\eta = 10$ dB
	$K_R = 3$, $L = 30$
Computation model	$V_k = [200, 300]$ Kb
	$c_k = [500, 600]$ cycle/bit
	$f_k^l = [1 \times 10^8, 2 \times 10^8]$ cycle/s
	$f_{\text{total}}^e = 5 \times 10^{10}$ cycle/s
Weight	$\xi_k = 1/K$
Convergence criterion	$\epsilon = 10^{-3}$

(NLoS) component. The LoS component $\tilde{\mathbf{H}}_{\text{LoS}}$ is modeled as $\tilde{\mathbf{H}}_{\text{LoS}} = \mathbf{a}_r(\theta^{AoA}) \mathbf{a}_t^H(\theta^{AoD})$, where the steering vectors w.r.t. the angle of arrival (AoA) θ^{AoA} and the angle of departure (AoD) θ^{AoD} are given by

$$\begin{aligned} \mathbf{a}_r(\theta^{AoA}) &= [1, e^{j\frac{2\pi d}{\lambda} \sin \theta^{AoA}}, \dots, e^{j\frac{2\pi d}{\lambda} (D_r-1) \sin \theta^{AoA}}]^T, \\ \mathbf{a}_t(\theta^{AoD}) &= [1, e^{j\frac{2\pi d}{\lambda} \sin \theta^{AoD}}, \dots, e^{j\frac{2\pi d}{\lambda} (D_t-1) \sin \theta^{AoD}}]^T. \end{aligned} \quad (68)$$

In (68), D_r and D_t represent the numbers of antennas at the receiver side and the transmitter side, respectively, and parameters d and λ denote the antenna spacing and wavelength, respectively. For simplicity, we set $d/\lambda = 1/2$. The detailed settings of the above parameters are specified in the ‘‘Communication and Radar model’’ block and the computing parameters V_k , c_k , f_k^l and f_{total}^e are specified in the ‘‘Computation model’’ block of Table I.

In the subsequent subsections, we evaluate our proposed algorithms against the benchmark schemes listed below:

- **RandPhase**: Assuming that the RIS phase shifts are randomly generated following a uniform distribution from 0 to 2π , we jointly optimize the precoding and decoding matrices of UEs, the offloading volume, and the edge computational resource allocation. This optimization is conducted according to Algorithm 5 and Algorithm 4 in the single-UE and multi-UE scenarios, respectively, while excluding the design of the RIS phase shift.
- **Without RIS**: The RIS-UE links are assumed to be blocked. Only the precoding and decoding matrices of UEs, along with the offloading volume and the edge computational resource allocation, are jointly optimized using Algorithm 5 and Algorithm 4 in the single-UE and multi-UE scenarios, respectively.

Fig. 3 presents the weighted latency versus the number of iterations for various numbers of RIS reflecting elements, i.e. $L = 10$, $L = 30$, and $L = 50$, in both single-UE and multi-UE scenarios. It can be seen from Fig. 3 that as the number of reflecting elements increases, the latency decreases due to the strengthened RIS-related link. Furthermore, both the proposed algorithms demonstrate rapid convergence within 5 iterations.

Fig. 4 illustrates the algorithm performance under different initialization settings in both single-UE and multi-UE

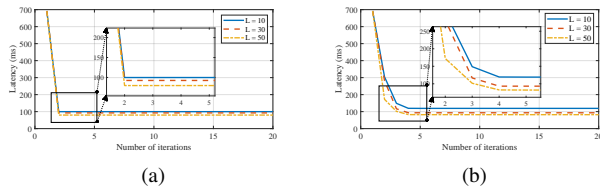


Fig. 3. Convergence behavior of the proposed algorithm for (a) the single-UE scenario using Algorithm 5 and (b) the multi-UE scenario using Algorithm 4.

scenarios. We consider 10 channel realizations and parameters for random computational tasks, labeled 1 - 10. For each specific generation of channels and computational tasks, we randomly initialize the optimization variables 100 times and subsequently calculate the corresponding solutions using the algorithm outlined in the preceding section. Within these 100 result sets, the maximum latency, denoted by **Max**, represents the worst solution obtained from the algorithm, while the minimum latency, approximating the global optimal value, is designated as **Min**, as depicted in Fig. 4. Notably, in the single-UE scenario, the values of **Max** and **Min** are similar, suggesting a high probability of achieving the globally optimal solution. In the multi-UE scenario, the maximum deviation is 5.6%, indicating that the solutions generated by the proposed algorithm closely approach the optimal solution.

Fig. 5 depicts the weighted latency versus the number of RIS elements. In addition to the three aforementioned benchmark schemes, we also explore two scenarios where the continuous RIS phase shifts are quantized to 1 and 2 bits due to the practical hardware constraints. Specifically, in the **With RIS, 1 bit** scheme, the phase shift of RIS elements is limited to either 0 or π , whereas the **With RIS, 2 bit** scheme offers four options: $\{0, \frac{\pi}{2}, \pi, \frac{3\pi}{2}\}$. Our observations yield the following insights. Firstly, the latency of the **RandPhase** scheme exhibits a gradual decrease w.r.t. the number of RIS elements, widening the gap with the **Without RIS** scheme. This suggests that integrating RIS can enhance communication performance even in the absence of intricate phase shift designs for the RIS elements. Secondly, the performance improvement of the **With RIS** scheme over the **RandPhase** scheme is observed to amplify with the increase of RIS elements. This observation underscores the significance of meticulously designing the phase-shift response of RIS for enhancing beamforming gain with an increasing number of RIS elements. Finally, in comparison to the **With RIS, 1 bit** scheme, the latency in the **With RIS, 2 bit** scheme is reduced and approaches the levels observed in the continuous phase shift scheme **With RIS**. This finding suggests that considering continuous phase design can serve as a tight bound for evaluating the practical discrete RIS phase shift configuration.

Fig. 6 plots the weighted latency versus the path loss exponent associated with RIS, specifically α_{ru} and α_r , which are designated as α_{RIS} , under different offloading strategies. It can be seen from Fig. 6 that as expected, the latency escalates w.r.t. α_{RIS} . In addition, the latency in the **RandPhase**

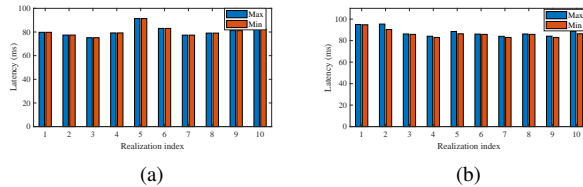
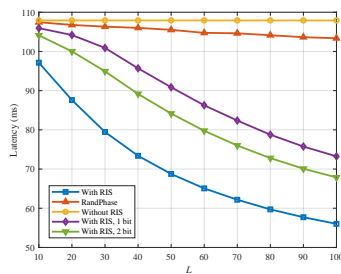


Fig. 4. Simulation results of the maximum and minimum latency versus the realization index obtained under 100 random initialization settings for (a) the single-UE scenario using Algorithm 5 and (b) the multi-UE scenario using Algorithm 4.

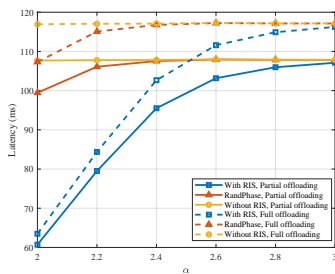
scheme closely resembles that of the **Without RIS** scheme when the value of α_{RIS} is substantial. This is because the beamforming gain introduced by the RIS cannot compensate for an increasing channel path-loss α_{RIS} and the direct UE-BS links are dominated. This implies that in practical applications, strategic placement of the RIS is crucial to circumvent obstacles and achieve reduced values of α_r and α_{ru} . Additionally, we examine the influence of offloading strategies. The latency achieved with the partial offloading strategy is smaller than that with the full offloading strategy, and the disparity between the two strategies is widened as α_r increases. The reason for this discrepancy can be explained as follows. In scenarios with favorable channel conditions, both strategies tend to offload the computational task to the edge server. However, as the RIS-related channel deteriorates, the partial offloading strategy becomes smarter in the processing part of the computational task locally.

Fig. 7 shows the weighted latency versus the edge computing capability under different numbers of transmit and receive antennas. The latency initially decreases significantly as the processing rate of the ECS f_{total}^e rises, followed by a deceleration in the rate of latency reduction. This is because at lower f_{total}^e values, the latency is primarily influenced by edge computing capability. By contrast, at higher f_{total}^e levels, the computation offloading delay is dominant in the overall latency. As a result, minimizing latency does not necessarily require equipping edge computing nodes with excessively powerful computational capabilities. Furthermore, a noteworthy decrease in latency occurs with an increase in the numbers of transmit and receive antennas, especially in the multi-UE scenario.

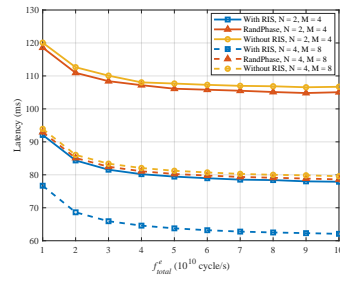
Fig. 8 portrays the weighted latency versus the SNR(SINR) threshold η . In the single-UE scenario, latency remains relatively constant despite variations in the threshold, whereas in multi-UE scenarios, latency increases with η . As demonstrated in Appendix B, the design of the optimal waveform essentially involves power allocation between the radar target and the BS. When the radar SNR requirement is low, there is no necessity to allocate power specifically for the radar target, as the signal transmitted to the BS inherently provides sufficient power to adequately meet the SNR requirement for the radar target. In a similar vein, within multi-UE scenarios, interference generated by other UEs necessitates the allocation of additional power to radar sensing in order to maintain the efficiency constraint (η), consequently resulting in an increase in latency.



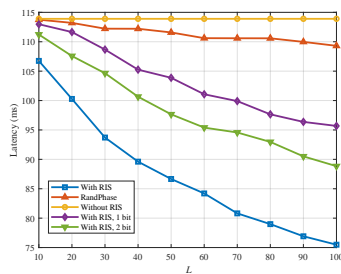
(a)



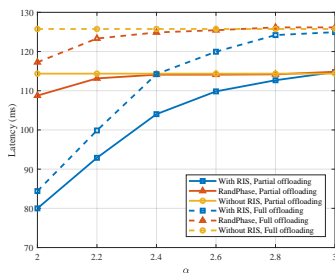
(a)



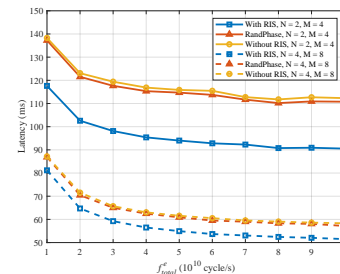
(a)



(b)



(b)



(b)

Fig. 5. Latency versus the number of RIS elements for (a) the single-UE scenario using Algorithm 5 and (b) the multi-UE scenario using Algorithm 4.

Fig. 6. Latency versus the α_{RIS} path loss exponent for (a) the single-UE scenario using Algorithm 5 and (b) the multi-UE scenario using Algorithm 4.

Fig. 7. Latency versus the edge computing capability for (a) the single-UE scenario using Algorithm 5 and (b) the multi-UE scenario using Algorithm 4.

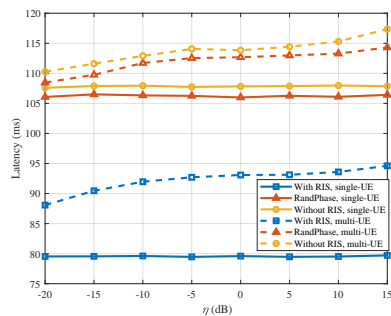


Fig. 8. Latency versus the SNR threshold for the single-UE scenario using Algorithm 5 and the SINR threshold for the multi-UE scenario using Algorithm 4.

VI. CONCLUSION

In this paper, we investigated a framework for RIS-assisted ICSC systems with a User-centric focus, aimed at enhancing the performance of DFRC-enabled UEs. A latency minimization problem was formulated by jointly optimizing the precoding and decoding matrices of the uplink signal, the receive radar beamforming vector, the RIS phase shift vector, the offloading volume, and the edge computational resource allocation in both multi-UE scenario and single-UE scenario. In the multi-UE scenario, we proposed an algorithm based on the BCD method to address the non-convexity of the problem by optimizing the computational and beamforming settings alternately. Specifically, for the computational settings, a closed-form solution for the offloading volume was derived, and a low-complexity algorithm based on the bisection

search method was applied to enhance the optimization of edge computing resource allocation. Then, two equivalent transformations were applied to the active and passive beamforming matrices to convert the OF, originally expressed as a non-convex sum-of-ratios, into a weighted sum-rate form, which was tackled by using a pair of efficient algorithms. Moreover, a low complexity algorithm with closed-form solutions was provided in the simplified single-UE scenario. Simulation results indicated a significant performance enhancement in latency with the proposed algorithm compared to the conventional approach operating without the integration of an RIS. Furthermore, numerical analysis confirmed the efficiency of our proposed algorithm.

APPENDIX A

THE PROOF OF PROPOSITION 1

The partial Lagrange function of Problem $\mathcal{P}2$ -1 is given by

$$\mathcal{L}(\mathbf{F}_c, \mathbf{W}_c, \boldsymbol{\theta}, \boldsymbol{\lambda}) = \sum_{k=1}^K \lambda_k + \sum_{k=1}^K \delta_k [\xi_k v_k - \lambda_k R_k(\mathbf{F}_c, \mathbf{W}_c, \boldsymbol{\theta})], \quad (\text{A.1})$$

where $\{\delta_k\}$ is the Lagrange multiplier. Given that $\{\mathbf{F}_c^*, \mathbf{W}_c^*, \mathbf{w}_s^*, \boldsymbol{\theta}^*, \boldsymbol{\lambda}^*\}$ represents the solution to Problem $\mathcal{P}2$ -1, there exists $\boldsymbol{\delta}^*$ that fulfills the following KKT conditions:

$$\frac{\partial \mathcal{L}}{\partial \theta_k} = -\delta_k^* \lambda_k^* \nabla R_k(\mathbf{F}_c^*, \mathbf{W}_c^*, \boldsymbol{\theta}^*) = 0, \forall k \in \mathcal{K}, \quad (\text{A.2})$$

$$\frac{\partial \mathcal{L}}{\partial F_{c,k}} = -\delta_k^* \lambda_k^* \nabla R_k(\mathbf{F}_c^*, \mathbf{W}_c^*, \boldsymbol{\theta}^*) = 0, \forall k \in \mathcal{K}, \quad (\text{A.3})$$

$$\frac{\partial \mathcal{L}}{\partial W_{c,k}} = -\delta_k^* \lambda_k^* \nabla R_k(\mathbf{F}_c^*, \mathbf{W}_c^*, \boldsymbol{\theta}^*) = 0, \forall k \in \mathcal{K}, \quad (\text{A.4})$$

$$\frac{\partial \mathcal{L}}{\partial \lambda_k} = 1 - \delta_k^* R_k(\mathbf{F}_c^*, \mathbf{W}_c^*, \boldsymbol{\theta}^*) = 0, \forall k \in \mathcal{K}, \quad (\text{A.5})$$

$$\delta_k^* [\xi_k v_k - \lambda_k^* R_k(\mathbf{F}_c^*, \mathbf{W}_c^*, \boldsymbol{\theta}^*)] = 0, \forall k \in \mathcal{K}, \quad (\text{A.6})$$

$$\delta_k^* \geq 0, \forall k \in \mathcal{K}, \quad (\text{A.7})$$

$$\xi_k v_k - \lambda_k^* R_k(\mathbf{F}_c^*, \mathbf{W}_c^*, \boldsymbol{\theta}^*) \leq 0, \forall k \in \mathcal{K}, \quad (\text{A.8})$$

$$0 \leq \theta_k^* \leq 2\pi, \forall k \in \mathcal{K}. \quad (\text{A.9})$$

Since $R_k(\mathbf{F}_c, \boldsymbol{\theta}) > 0$, (A.5) is equivalent to

$$\delta_k^* = \frac{1}{R_k(\mathbf{F}_c^*, \mathbf{W}_c^*, \boldsymbol{\theta}^*)}, \forall k \in \mathcal{K}. \quad (\text{A.10})$$

From (A.6), we can derive that

$$\lambda_k^* = \frac{\xi_k v_k}{R_k(\mathbf{F}_c^*, \mathbf{W}_c^*, \boldsymbol{\theta}^*)}, \forall k \in \mathcal{K}. \quad (\text{A.11})$$

When we set $\boldsymbol{\lambda} = \boldsymbol{\lambda}^*$ and $\boldsymbol{\delta} = \boldsymbol{\delta}^*$, the KKT conditions of Problem $\mathcal{P}2$ -2 are the same as (A.2), (A.3), (A.4), and (A.9). Thus, Proposition 1 is proved.

APPENDIX B THE PROOF OF PROPOSITION 2

First, we demonstrate that when the OF of Problem $\mathcal{P}3$ -3 is maximized, the constraint in (59b) achieves the upper bound $\mathbf{f}_c \mathbf{f}_c^H = P_t$ by using the proof by contradiction. Assuming that \mathbf{f}_c^* represents the optimal solution of Problem $\mathcal{P}3$ -3 such that $\mathbf{f}_c^* \mathbf{f}_c^{*H} < P_t$, we can derive $\hat{\mathbf{f}}_c = (1 + \beta) \mathbf{f}_c^*$ satisfying $\hat{\mathbf{f}}_c \hat{\mathbf{f}}_c^H = P_t$, where $\beta \geq 0$, as a feasible solution of Problem $\mathcal{P}3$ -3. Since the OF of Problem $\mathcal{P}3$ -3 when $\mathbf{f}_c = \hat{\mathbf{f}}_c$ surpasses that when $\mathbf{f}_c = \mathbf{f}_c^*$, the OF of Problem $\mathcal{P}3$ -3 is maximized if and only if when $\mathbf{f}_c \mathbf{f}_c^H = P_t$. Thus, Problem $\mathcal{P}3$ -3 can be rewritten as

$$\max_{\mathbf{f}_c} \left| \mathbf{h}^H \mathbf{f}_c \right|^2 \quad (\text{B.1a})$$

$$s.t. \quad |\mathbf{f}_c|^2 = P_t, \quad (\text{B.1b})$$

$$|\mathbf{g}^H \mathbf{f}_c|^2 \geq \eta. \quad (\text{B.1c})$$

If $\eta > P_t \|\mathbf{g}\|^2$, by applying the Cauchy's inequality, we have $|\mathbf{g}^H \mathbf{f}_c|^2 \leq \|\mathbf{g}\|^2 \|\mathbf{f}_c\|^2 = P_t \|\mathbf{g}\|^2 < \eta$, which is in conflict with constraint (B.1c). Thus, Problem (B.1) is feasible only when $\eta \leq P_t \|\mathbf{g}\|^2$. Case 3 in Proposition 2 is proved.

As Problem (B.1) is convex and satisfies Slater's condition [33], the KKT conditions are utilized to address this problem. The Lagrange function of Problem (B.1) is expressed as

$$\mathcal{L}(\mathbf{f}_c) = -\mathbf{h}^H \mathbf{f}_c \mathbf{f}_c^H \mathbf{h} + \varphi(\eta - \mathbf{g}^H \mathbf{f}_c \mathbf{f}_c^H \mathbf{g}) + \iota(\mathbf{f}_c \mathbf{f}_c^H - P_t), \quad (\text{B.2})$$

where φ and ι are the Lagrange multipliers. Then, the KKT conditions for (B.1) can be formulated as follows:

$$\frac{\partial \mathcal{L}}{\partial \mathbf{f}_c^*} = -\mathbf{h}^H \mathbf{f}_c \mathbf{h} - \varphi \mathbf{g}^H \mathbf{f}_c \mathbf{g} + \iota \mathbf{f}_c = \mathbf{0}, \quad (\text{B.3})$$

$$\eta - \mathbf{g}^H \mathbf{f}_c \mathbf{f}_c^H \mathbf{g} \leq 0, \quad (\text{B.4})$$

$$\mathbf{f}_c \mathbf{f}_c^H - P_t = 0, \quad (\text{B.5})$$

$$\varphi \geq 0, \quad (\text{B.6})$$

$$\varphi(\eta - \mathbf{g}^H \mathbf{f}_c \mathbf{f}_c^H \mathbf{g}) = 0. \quad (\text{B.7})$$

(B.3) is equivalent to

$$\mathbf{f}_c = \frac{\mathbf{h}^H \mathbf{f}_c}{\iota} \mathbf{h} + \frac{\varphi \mathbf{g}^H \mathbf{f}_c}{\iota} \mathbf{g}, \quad (\text{B.8})$$

which indicates $\mathbf{f}_c \in \text{span}(\mathbf{h}, \mathbf{g})$. For convenience, \mathbf{f}_c can be rewritten as

$$\mathbf{f}_c = a\mathbf{h} + b\mathbf{g}, \quad (\text{B.9})$$

where the coefficients a and b denote the amplitudes of the power budget allocated to communication and radar sensing, respectively. By substituting (B.9) into (B.5), we obtain that

$$|a|^2 \mathbf{h}^H \mathbf{h} + a^* b \mathbf{h}^H \mathbf{g} + ab^* \mathbf{g}^H \mathbf{h} + |b|^2 \mathbf{g}^H \mathbf{g} = P_t. \quad (\text{B.10})$$

Moreover, (B.7) suggests that either φ or $\eta - \mathbf{g}^H \mathbf{f}_c \mathbf{f}_c^H \mathbf{g}$ equals to 0. Next, we discuss the different cases separately.

1) When $\varphi = 0$, (B.8) is transformed into

$$\mathbf{f}_c = \frac{\mathbf{h}^H \mathbf{f}_c}{\iota} \mathbf{h}. \quad (\text{B.11})$$

By substituting (B.9) into (B.11), we derive that

$$a\mathbf{h} + b\mathbf{g} = \frac{a\mathbf{h}^H \mathbf{h} + b\mathbf{h}^H \mathbf{g}}{\iota} \mathbf{h}. \quad (\text{B.12})$$

From (B.12), it can be deduced that $b = 0$. By substituting $b = 0$ into (B.10), the value of a can be determined as

$$|a| = \frac{\sqrt{P_t}}{\|\mathbf{h}\|}, \quad (\text{B.13})$$

where the phase of a is arbitrary. Meanwhile, it can be derived from (B.4) that

$$\eta \leq \frac{P_t |\mathbf{g}^H \mathbf{h}|^2}{\|\mathbf{h}\|^2}. \quad (\text{B.14})$$

Thus, Case 1 in Proposition 2 is proved.

2) When $\eta - \mathbf{g}^H \mathbf{f}_c \mathbf{f}_c^H \mathbf{g} = 0$, by substituting (B.9) into $\eta - \mathbf{g}^H \mathbf{f}_c \mathbf{f}_c^H \mathbf{g} = 0$ and (B.8), we have

$$|a|^2 \mathbf{g}^H \mathbf{h} \mathbf{h}^H \mathbf{g} + a^* b \mathbf{g}^H \mathbf{g} \mathbf{h}^H \mathbf{g} + ab^* \mathbf{g}^H \mathbf{h} \mathbf{g}^H \mathbf{g} + |b|^2 \mathbf{g}^H \mathbf{g} \mathbf{g}^H \mathbf{g} = \eta, \quad (\text{B.15})$$

$$a\mathbf{h} + b\mathbf{g} = \frac{a\mathbf{h}^H \mathbf{h} + b\mathbf{h}^H \mathbf{g}}{\iota} \mathbf{h} + \frac{\varphi(a\mathbf{g}^H \mathbf{h} + b\mathbf{g}^H \mathbf{g})}{\iota} \mathbf{g}. \quad (\text{B.16})$$

From (B.10) and (B.15), it can be derived that

$$|a| = \sqrt{\frac{P_t \|\mathbf{g}\|^2 - \eta}{\|\mathbf{h}\|^2 \|\mathbf{g}\|^2 - |\mathbf{h}^H \mathbf{g}|^2}}. \quad (\text{B.17})$$

From (B.16), we obtain that

$$\angle(a) = \angle(a\mathbf{h}^H \mathbf{h} + b\mathbf{h}^H \mathbf{g}) = \angle(b\mathbf{h}^H \mathbf{g}), \quad (\text{B.18})$$

$$\angle(b) = \angle(a\mathbf{g}^H \mathbf{h} + b\mathbf{g}^H \mathbf{g}) = \angle(a\mathbf{g}^H \mathbf{h}). \quad (\text{B.19})$$

It follows

$$\angle(a) - \angle(b) = \angle(\mathbf{h}^H \mathbf{g}). \quad (\text{B.20})$$

Meanwhile, by substituting (B.17) and (B.20) into (B.10), we derive that

$$|b| = \frac{\sqrt{\eta}}{\|\mathbf{g}\|^2} - \frac{|\mathbf{h}^H \mathbf{g}|}{\|\mathbf{g}\|^2} |a|. \quad (\text{B.21})$$

Furthermore, since $|b| \geq 0$, the parameter η satisfies $\eta \geq \frac{P_t |\mathbf{g}^H \mathbf{h}|^2}{\|\mathbf{h}\|^2}$. Thus, Case 2 in Proposition 2 is proved.

REFERENCES

- [1] J. Wan, H. Ren, C. Pan, Z. Yu, Z. Zhang, and Y. Zhang, "Reconfigurable intelligent surface assisted integrated sensing, communication and computation systems," in *Proc. 2024 IEEE Int. Conf. Acoust. Speech Signal Process. Workshops (ICASSPW)*, Apr. 2024, pp. 189–193.
- [2] D. K. Pin Tan, J. He, Y. Li, A. Bayesteh, Y. Chen, P. Zhu, and W. Tong, "Integrated sensing and communication in 6G: Motivations, use cases, requirements, challenges and future directions," in *Proc. 2021 1st IEEE Int. Online Symp. Joint Commun. & Sensing (JC&S)*, Feb. 2021, pp. 1–6.
- [3] A. Liu, Z. Huang, M. Li, Y. Wan, W. Li, T. X. Han, C. Liu, R. Du, D. K. P. Tan, J. Lu, Y. Shen, F. Colone, and K. Chetty, "A survey on fundamental limits of integrated sensing and communication," *IEEE Commun. Surv. Tuts.*, vol. 24, no. 2, pp. 994–1034, Feb. 2022.
- [4] R. Liu, M. Li, Y. Liu, Q. Wu, and Q. Liu, "Joint transmit waveform and passive beamforming design for RIS-aided DFRC systems," *IEEE J. Sel. Top. in Signal Process.*, vol. 16, no. 5, pp. 995–1010, May 2022.
- [5] A. Hassani, M. G. Amin, Y. D. Zhang, and F. Ahmad, "Dual-function radar-communications: Information embedding using sidelobe control and waveform diversity," *IEEE Trans. Signal Process.*, vol. 64, no. 8, pp. 2168–2181, Dec. 2016.
- [6] S. Bi and Y. Zhang, "Computation rate maximization for wireless powered mobile-edge computing with binary computation offloading," *IEEE Trans. Wireless Commun.*, vol. 17, no. 6, pp. 4177–4190, Jun. 2018.
- [7] Z. Wang, Y. Wei, Z. Feng, F. R. Yu, and Z. Han, "Resource management and reflection optimization for intelligent reflecting surface assisted multi-access edge computing using deep reinforcement learning," *IEEE Trans. Wireless Commun.*, vol. 22, no. 2, pp. 1175–1186, Feb. 2023.
- [8] D. Wen, P. Liu, G. Zhu, Y. Shi, J. Xu, Y. C. Eldar, and S. Cui, "Task-oriented sensing, computation, and communication integration for multi-device edge AI," *IEEE Trans. Wireless Commun.*, pp. 1–1, Aug. 2023.
- [9] J. A. Zhang, M. L. Rahman, K. Wu, X. Huang, Y. J. Guo, S. Chen, and J. Yuan, "Enabling joint communication and radar sensing in mobile networks—a survey," *IEEE Commun. Surv. Tuts.*, vol. 24, no. 1, pp. 306–345, Oct. 2022.
- [10] X. Chen, Z. Feng, J. A. Zhang, Z. Yang, X. Yuan, X. He, and P. Zhang, "Integrated communication, sensing, and computation framework for 6G networks," 2023, [Online]. Available: <https://arxiv.org/abs/2310.03265>.
- [11] X. Li, F. Liu, Z. Zhou, G. Zhu, S. Wang, K. Huang, and Y. Gong, "Integrated sensing, communication, and computation over-the-air: MIMO beamforming design," *IEEE Trans. Wireless Commun.*, vol. 22, no. 8, pp. 5383–5398, Aug. 2023.
- [12] Z. Peng, R. Weng, Z. Zhang, C. Pan, and J. Wang, "Active reconfigurable intelligent surface for mobile edge computing," *IEEE Wireless Commun. Lett.*, vol. 11, no. 12, pp. 2482–2486, Sep. 2022.
- [13] X. Wang, Z. Fei, J. Huang, and H. Yu, "Joint waveform and discrete phase shift design for RIS-assisted integrated sensing and communication system under cramer-rao bound constraint," *IEEE Trans. Veh. Technol.*, vol. 71, no. 1, pp. 1004–1009, Oct. 2022.
- [14] Y. Guo, Y. Liu, Q. Wu, X. Li, and Q. Shi, "Joint beamforming and power allocation for RIS aided full-duplex integrated sensing and uplink communication system," *IEEE Trans. Wireless Commun.*, pp. 1–1, 2023.
- [15] T. Wu, C. Pan, K. Zhi, H. Ren, M. ElKashlan, J. Wang, and C. Yuen, "Employing high-dimensional RIS information for RIS-aided localization systems," *IEEE Commun. Lett.*, pp. 1–1, Jul. 2024.
- [16] T. Wu, C. Pan, K. Zhi, H. Ren, M. ElKashlan, C. Wang, R. Schober, and X. You, "Exploit high-dimensional RIS information to localization: What is the impact of faulty element?" *IEEE J. Sel. Areas Commun.*, pp. 1–1, Jun. 2024.
- [17] Y. Zhang, H. Ren, C. Pan, B. Wang, Z. Yu, R. Weng, T. Wu, and Y. He, "Secure wireless communication in active ris-assisted dfrc systems," *IEEE Trans. Veh. Technol.*, pp. 1–15, 2024.
- [18] Z. Jiang, M. Rihan, P. Zhang, L. Huang, Q. Deng, J. Zhang, and E. M. Mohamed, "Intelligent reflecting surface aided dual-function radar and communication system," *IEEE Syst. J.*, vol. 16, no. 1, pp. 475–486, Mar. 2022.
- [19] G. Zhang, C. Shen, F. Liu, Y. Lin, and Z. Zhong, "Beampattern design for RIS-Aided dual-functional radar and communication systems," in *Proc. 2022 IEEE Global Commun. Conf. (GLOBECOM)*, Dec. 2022, pp. 3899–3904.
- [20] K. Zhi, C. Pan, H. Ren, K. Chai, and M. ElKashlan, "Active RIS versus passive RIS: Which is superior with the same power budget?" *IEEE Commun. Lett.*, vol. 26, no. 5, pp. 1150–1154, May 2022.
- [21] C. Pan, G. Zhou, K. Zhi, S. Hong, T. Wu, Y. Pan, H. Ren, M. D. Renzo, A. Lee S., R. Zhang, and A. Y. Zhang, "An overview of signal processing techniques for RIS/IRS-aided wireless systems," *IEEE J. Sel. Top. Signal Process.*, vol. 16, no. 5, pp. 883–917, Aug. 2022.
- [22] T. Bai, C. Pan, Y. Deng, M. ElKashlan, A. Nallanathan, and L. Hanzo, "Latency minimization for intelligent reflecting surface aided mobile edge computing," *IEEE J. Sel. Areas Commun.*, vol. 38, no. 11, pp. 2666–2682, Jul. 2020.
- [23] N. Huang, T. Wang, Y. Wu, Q. Wu, and T. Q. S. Quek, "Integrated sensing and communication assisted mobile edge computing: An energy-efficient design via intelligent reflecting surface," *IEEE Wireless Commun. Lett.*, vol. 11, no. 10, pp. 2085–2089, Jul. 2022.
- [24] S. Xu, Y. Du, J. Zhang, J. Liu, J. Wang, and J. Zhang, "Intelligent reflecting surface enabled integrated sensing, communication and computation," *IEEE Trans. Wireless Commun.*, pp. 1–1, Jul. 2023.
- [25] Y. He, G. Yu, Y. Cai, and H. Luo, "Integrated sensing, computation, and communication: System framework and performance optimization," *IEEE Trans. Wireless Commun.*, pp. 1–1, Jun. 2023.
- [26] N. Huang, C. Dou, Y. Wu, L. Qian, B. Lin, and H. Zhou, "Unmanned-aerial-vehicle-aided integrated sensing and computation with mobile-edge computing," *IEEE Internet Things J.*, vol. 10, no. 19, pp. 16830–16844, Apr. 2023.
- [27] N. Huang, C. Dou, Y. Wu, L. Qian, and R. Lu, "Energy-efficient integrated sensing and communication: A multi-access edge computing design," *IEEE Wireless Commun. Lett.*, pp. 1–1, Aug. 2023.
- [28] C. Ding, J. Wang, H. Zhang, M. Lin, and G. Y. Li, "Joint MIMO precoding and computation resource allocation for dual-function radar and communication systems with mobile edge computing," *IEEE J. Sel. Areas Commun.*, vol. 40, no. 7, pp. 2085–2102, Mar. 2022.
- [29] Z. Yu, H. Ren, C. Pan, G. Zhou, B. Wang, M. Dong, and J. Wang, "Active RIS aided ISAC systems: Beamforming design and performance analysis," *IEEE Trans. Commun.*, pp. 1–1, Nov. 2023.
- [30] J. Xiao, J. Tang, and J. Chen, "Efficient radar detection for RIS-aided dual-functional radar-communication system," in *2023 IEEE 97th Vehicular Technology Conference (VTC2023-Spring)*, Jun. 2023, pp. 1–6.
- [31] R. P. Sankar, S. P. Chepuri, and Y. C. Eldar, "Beamforming in integrated sensing and communication systems with reconfigurable intelligent surfaces," *IEEE Trans. Wireless Commun.*, pp. 1–1, Sep. 2023.
- [32] M. Bennis, M. Debbah, and H. V. Poor, "Ultrareliable and low-latency wireless communication: Tail, risk, and scale," *Proc. IEEE*, vol. 106, no. 10, pp. 1834–1853, Oct. 2018.
- [33] S. Boyd and L. Vandenberghe, *Convex Optimization*. Cambridge, U.K.: Cambridge Univ. Press, 2004.
- [34] C. Pan, H. Ren, K. Wang, M. ElKashlan, A. Nallanathan, J. Wang, and L. Hanzo, "Intelligent reflecting surface aided MIMO broadcasting for simultaneous wireless information and power transfer," *IEEE J. Sel. Areas Commun.*, vol. 38, no. 8, pp. 1719–1734, Aug. 2020.
- [35] Y. Jong, "An efficient global optimization algorithm for nonlinear sum-of-ratios problem," *Optimization Online*, pp. 1–21, 2012.
- [36] Q. Shi, M. Razaviyayn, Z. Luo, and C. He, "An iteratively weighted MMSE approach to distributed sum-utility maximization for a MIMO interfering broadcast channel," in *Proc. 2011 IEEE Int. Conf. Acoust. Speech Signal Process. (ICASSP)*, Jul. 2011, pp. 3060–3063.
- [37] J. Capon, "High-resolution frequency-wavenumber spectrum analysis," *Proc. IEEE Inst. Electr. Electron. Eng.*, vol. 57, no. 8, pp. 1408–1418, Aug. 1969.
- [38] M. Grant and S. Boyd, "CVX: Matlab software for disciplined convex programming, version 2.1," 2014.
- [39] Y. Sun, P. Babu, and P. Palomar, "Majorization-minimization algorithms in signal processing, communications, and machine learning," *IEEE Trans. Signal Process.*, vol. 65, no. 3, pp. 794–816, Feb. 2017.
- [40] C. Pan, H. Ren, K. Wang, W. Xu, M. ElKashlan, A. Nallanathan, and L. Hanzo, "Multicell MIMO communications relying on intelligent reflecting surfaces," *IEEE Trans. Wireless Commun.*, vol. 19, no. 8, pp. 5218–5233, Aug. 2020.
- [41] A. Bazzi and M. Chafii, "On outage-based beamforming design for dual-functional radar-communication 6G systems," *IEEE Trans. Wireless Commun.*, vol. 22, no. 8, pp. 5598–5612, Aug. 2023.
- [42] Z. Zheng, X. Liu, T. Huang, Y. Liu, and Y. Eldar, "Towards a performance bound on MIMO DFRC systems," 2022, [Online]. Available: <https://arxiv.org/abs/2211.06979>.